THESIS

RELATIONSHIPS BETWEEN SOIL ORGANIC CARBON STORAGE AND INUNDATION DYNAMICS IN HEADWATER FLOODPLAINS

Submitted by

Mariah Papac

Department of Civil and Environmental Engineering

In partial fulfillment of requirements

For the Degree of Master of Science

Colorado State University

Fort Collins, Colorado

Summer 2026

Master's Committee:

Advisor: Ryan Morrison

Danny White
Ellen Wohl

ABSTRACT

RELATIONSHIPS BETWEEN SOIL ORGANIC CARBON STORAGE AND INUNDATION DYNAMICS IN HEADWATER FLOODPLAINS

Floodplains serve as carbon storage hotspots where periodic inundation supports vegetation growth, nutrient-rich sediment deposition, and organic matter accumulation. Headwater floodplains, in particular, store substantial amounts of soil organic carbon (SOC) relative to their watershed area. However, the relationship between inundation dynamics (e.g., inundation frequency) and floodplain SOC content remains poorly understood. I hypothesized that SOC accumulation would follow a non-linear response to floodplain inundation, with intermediate inundation recurrence intervals yielding the highest carbon storage.

To test this hypothesis, I collected floodplain soil cores from three headwater rivers in the Colorado Rockies: Little Beaver Creek, Lower Elkhorn Creek, and the Laramie River. All three floodplain reaches were slated for restoration to improve lateral connectivity with the floodplain. The coring locations were randomly chosen based on pre-selected surface elevation bins relative to the channel. I processed the floodplain samples, which included organic layer and mineral samples. I calculated each mineral sample's bulk density and measured its carbon content using an elemental analyzer. I then created two-dimensional steady-state hydrodynamic models for each floodplain reach and simulated the 2-, 5-, 10-, 25-, 50-, 100-, 200-, and 500-yr recurrence interval discharges. I grouped cores based on their initial inundation discharge to determine whether frequency of inundation (i.e., cores flooded in the 2-yr recurrence interval discharge experienced the most frequent inundation) affected SOC storage.

I found surface elevation relative to the channel to be a weak predictor of SOC content and floodplain SOC stocks to be smaller than, but of comparable magnitude to, other Colorado headwater floodplains. For the relationship between SOC and inundation frequency, I found a bimodal distribution for Lower Elkhorn Creek and Laramie River, with the largest peak occurring for cores located in infrequently inundated areas (200- and 500-yr inundation) and the second peak occurring in frequently inundated areas (2- and 5-yr). Little Beaver Creek did not show the bimodal distribution due to a lack of cores located within the 2-, 5-, and 25-yr recurrence interval inundated areas. The bimodal results align with the few studies completed thus far to determine the relationship between inundation frequency and floodplain SOC. These studies were conducted on climatically different floodplains, but for the four floodplains studied, a single inundation regime, infrequent or frequent, corresponded with the greatest SOC storage. The conflicting results suggest that multiple processes may influence SOC storage with varying importance, depending on the floodplain. The disagreement between floodplains underscores the complex processes occurring in these systems and the importance of site-specific data collection to determine the efficacy of restoration if carbon sequestration is the goal.

ACKNOWLEDGEMENTS

This study was made possible through the funding from the Intermountain West Transformation Network, generously supported by the National Science Foundation under grant #2115169. It was completed in collaboration with the Rocky Mountain Research Station and the Coalition for the Poudre River Watershed.

I couldn’t have made it this far without the support from my family and friends. A huge thank you goes to my parents and partner, who provided support in every way over these last two years. Additionally, I am incredibly thankful for the support and mentorship provided by my advisor, Ryan Morrison. I appreciate the expertise and scientific guidance from Tim Fegel, Chuck Rhoades, Katherine Lininger, Taylor Johaneman, and my committee members Ellen Wohl and Danny White. I was supported extensively by Isabel McPherson in the lab and Madalena Fetter, Aleah Hahn, Alejandro Martinez, and Nick Christensen in the field. Thank you to my lab mates for the chats, reassurance, and research advice. This journey has been challenging, educational, and rewarding!

TABLE OF CONTENTS

LIST OF TABLES

LIST OF FIGURES

1. INTRODUCTION

1.1 Background

Floodplains are complex and highly dynamic alluvially shaped areas adjacent to river channels that are consistently flooded, home to specialized organisms, and the site of water, soil, and nutrient exchange (Junk et al., 1989; Nanson & Croke, 1992; Schmudde, 1968; Tockner & Stanford, 2002). The definition of a floodplain varies among disciplines, but all agree that floodplains are important ecosystems that are deteriorating due to anthropogenic stressors (Knox et al., 2022; Morrison et al., 2023). To help protect these important environments, people attempt to quantify their benefit to humanity. One such quantification method is the concept of ecosystem services (Fisher et al., 2009). Floodplains provide a plethora of ecosystem services, including:

- Attenuation of flood flows: floodplains store water in depressions and groundwater aquifers and possess significant hydraulic roughness (e.g., vegetation, surface topography) that allows for momentum exchange and energy loss in the flow, reducing the potential for downstream damage (Byrne et al., 2019; Christensen & Morrison, 2026; Hunt, 1990; Wohl, 2021; Woltemade & Potter, 1994);
- Groundwater storage: floodplain soils, characterized by layers of coarse and fine alluvial deposits, store groundwater from overbank flow and precipitation events. The groundwater storage supports base flows during the drier season providing downstream users water throughout the year (Hunt et al., 2018; Whiting & Pomeranets, 1997; Wohl, 2021);

- Nutrient and sediment capture: floodplains sit adjacent to river channels where overbank velocities are reduced, and suspended nutrient-rich fine sediments are deposited. Removing these particles from the water column improves water quality downstream (Hopkins et al., 2018; Wohl, 2021);
- Unique habitats: floodplains are characterized by disturbance-adapted riparian plants and animal species that find the specialized conditions necessary for their survival (Brown, 2002; Mahoney & Rood, 1998; Naiman & Décamps, 1997).

An ecosystem service not captured in the short list provided is the ability of floodplains to sequester carbon, which is the focus of this study.

The terrestrial carbon pool captures and sequesters large amounts of carbon, estimated at ~2500 Pg, second only to the oceanic pool (Gougoulias et al., 2014; Jobbágy & Jackson, 2000; Lal, 2008). Of the terrestrial carbon pools, soils make up the largest portion of carbon stores, in the form of organic and inorganic carbon (Lal, 2008). The amount of carbon stored in soils globally is difficult to quantify due to the complex interactions between physical, biological, and chemical processes that influence soil organic carbon (SOC) storage and/or release. These complex interactions, compounded by the unpredictability of future scenarios, make SOC storage difficult to predict (Intergovernmental Panel on Climate Change (IPCC), 2023; Schimel et al., 2001). Combinations of these factors result in certain ecosystems sequestering larger amounts of carbon than others. Floodplains serve as carbon hotspots due to seasonally variable water tables, periodic flood events that deposit organic matter (OM) and nutrient-rich sediment, and the presence of abundant living biomass (Cierjacks et al., 2010; Hinshaw & Wohl, 2023; Sutfin et al., 2016; Wohl et al., 2012). Specifically, the floodplains of headwater streams store substantial amounts of SOC that exceed those of other floodplains relative to their watershed area (Sutfin & Wohl, 2017). Headwater floodplains, therefore, are important to the terrestrial carbon budget.

Carbon cycling in floodplains is controlled, in large part, by flood flows that maintain soil moisture, recharge groundwater stores, and scour or deposit OM and sediments. It is crucial, therefore, to consider the flow regime of any floodplain to understand the dynamics of its SOC storage. The timing, frequency, duration, and rate of change of flow determine a river's natural flow regime and are important points of examination (Poff et al., 1997).

The moisture conditions of floodplains support abundant and variable growth of diverse vegetation (Naiman & Décamps, 1997). The vegetation's living biomass (above and belowground) and dead or decaying plant matter constitutes a large portion of the organic carbon stored on floodplains (Ruffing et al., 2016; Sutfin et al., 2016). Several studies suggest that floodplain vegetation may be the major contributor to floodplain SOC rather than allochthonous imports of sediment or organic matter (Hupp et al., 2019; Lininger et al., 2018; Scott & Wohl, 2018; Wohl et al., 2017). This vegetative carbon source is, however, spatially and temporally variable, as flood flows can redistribute the surficial plant matter across the floodplain, transport this autochthonous input downstream, scour away seedlings, and increase primary productivity (Sutfin et al., 2016; Wright et al., 2015).

Flow regime also governs groundwater storage, recharge, and release. When soil saturation conditions permit, floodplains experience groundwater recharge during flooding events. Soil moisture regulates root respiration and microbial decomposition of organic matter, with exceedingly dry or saturated conditions limiting the production of CO_2 (Annala et al., 2022; Rodrigues et al., 2023). Below the groundwater table, the soil is an anoxic environment. Anoxic conditions, characteristic of peatlands, inhibit microbial respiration and organic matter decomposition. These conditions alter the makeup of the microbial community resulting in less CO_2 release but an increased release of methane (Gougoulias et al., 2014; Ise et al., 2008). The methane released from the anoxic conditions has been found to contribute negligibly to the annual carbon balance in beaver-influenced wetlands (Hallberg et al., 2026). Soil moisture, therefore, plays a large role in SOC storage, which could be altered indirectly from climate change or directly through river and floodplain restoration

In addition to their effects on primary productivity and soil moisture, flood flows simultaneously deposit and scour away nutrient-rich sediments from the floodplain (Pinay et al., 1992). Floodplain sedimentation occurs due to increased surface roughness (e.g., topographic variability, density of vegetation) that reduces flow velocity thereby allowing suspended particles to deposit in a spatially variable manner (Walling & He, 1998). Depositional flood flow is an important contributor to floodplain SOC storage as shown by a positive correlation of SOC content with fine particle (clays) sedimentation. (Cheng et al., 2024; Graf-Rosenfellner et al., 2016; Hassink & Whitmore, 1997; Sutfin & Wohl, 2017; Yin et al., 2019).

1.2 Study Motivation

Few studies have analyzed the relationship between floodplain SOC storage and inundation frequency. Of the studies found, all were conducted on only four different wetlands/floodplains that all possess dissimilar characteristics from the small headwater river floodplains examined in this study. Bai and Yin's work was conducted in the Xianghai wetland (~175 m above sea level (ASL)) along the Huolin River (monsoonal climate conditions, 551.6 mm/yr precipitation) (2020 and 2019). Their study found that areas of higher SOC stocks occurred in more frequently flooded areas (Bai et al., 2020; Yin et al., 2019). Yin showed that the topsoils of the 5-yr floodplain experienced the highest SOC content (27.31 g/kg) while the permanently flooded subsurface soils exhibited the highest SOC content (10.87 g/kg). Hupp's work was completed along the Atchafalaya River (~50 m ASL) which experiences semi-arid continental monsoon climate conditions (~ 552 mm/yr precipitation) (Hupp et al., 2019). Hupp's study focused on the SOC source and found that autochthonous inputs from the riparian vegetation were the greatest contributor in all hydrogeomorphic regimes. Similar to Yin and Bai, Hupp (2019) found that areas frequently or permanently inundated had the highest SOC content. In contrast, Saint-Laurent and Gervais-Beaulac's studies showed that SOC content in frequently flooded soils was substantially lower than in the areas outside of flood zones (2014 and 2013). Their studies were conducted on the Saint-Francois (~115 m ASL) and Massawippi River, a tributary to the Saint-Francois River, which experience a cool and humid climate (~1,144 mm/yr precipitation) (Gervais-Beaulac, 2013; Saint-Laurent et al., 2014). The proposed relationships supporting the results found along the Huolin and Atchafalaya River, improved primary productivity and soil saturation increase SOC in frequently flooded areas, oppose those that support the results found along the Saint-Francois and Massawippi River, degradation of soils and diminished plant productivity due to frequent floodplain scour reduces SOC content. These conflicting results provide a glimpse of the complex conditions that interact to determine SOC in floodplains. The need for further research on the relationship between inundation dynamics and SOC storage in various floodplain settings is clear and supported by the results found in this study.

As floodplains are recognized as carbon hotspots (Sutfin et al., 2016; Wohl et al., 2012), they have received attention as a novel and ecological carbon-sequestration strategy. This recognition has gained traction, as State and Federal agencies have recently established greenhouse gas emission-reduction targets prompting the inception of carbon markets. These markets allow companies to offset their carbon emissions by purchasing credits. These credits can be generated by funding carbon-reduction projects or purchasing unused permits from another entity (UNDC, 2022). River and floodplain restoration with the intent to improve channel-floodplain connectivity has been proposed as a plausible carbon-sequestration strategy. However, with limited knowledge regarding the time scales and quantities of carbon sequestered in restored floodplain systems (Hinshaw & Wohl, 2023; Lininger & Lave, 2024; Matzek et al., 2015), providing carbon credits for river and floodplain restoration may be premature.

1.3 Study Objective

One effect of these proposed restoration projects is an increase in frequency and extent of floodplain inundation. However, the relationship between inundation dynamics and SOC accumulation is poorly understood. Furthering our understanding of the effects of inundation dynamics is critical to evaluate whether restoration strategies that increase the frequency and extent of inundation are effective at increasing carbon sequestration. This study aims to evaluate how inundation dynamics (e.g., relative elevation and inundation frequency/extent) affect floodplain SOC content in headwater floodplains. In addition, Hinshaw & Wohl (2023) suggest that the collection of pre- and post-restoration floodplain SOC data would provide results with less uncertainty than trying to compare sites with temporal and spatial variability. This study provides a valuable base-line dataset for future post-restoration comparisons at the studied floodplains.

I hypothesize that SOC accumulation will follow a non-linear response, with intermediate inundation recurrence intervals (10- through 50-yr) yielding the highest carbon storage. This hypothesis builds on established relationships between flood disturbance, soil moisture, and vegetation productivity at the two end members: areas flooded frequently, 2- through 5-yr recurrence intervals, and areas flooded infrequently, 100- through 500-yr recurrence intervals. Areas that are flooded frequently may be scoured, removing nutrient-rich sediment deposition and limiting plant recruitment (Mahoney & Rood, 1998; Saint-Laurent et al., 2014, 2016). However, areas that are flooded infrequently may not have the soil moisture content needed to reduce microbial respiration of CO_2 (Duan et al., 2018; Ise et al., 2008; Yin et al., 2019) or supplement groundwater stores that support abundant plant populations, which reduces OM inputs to soil (Merritt et al., 2010; Smith et al., 1991). Areas inundated at a frequency between these end members may experience an ideal combination of flood disturbance, soil moisture, and vegetation productivity that would result in the highest SOC content, see Figure 1 for a conceptual model that depicts the relationships that influenced the hypothesis. To test this hypothesis, SOC field data will be analyzed in conjunction with two-dimensional (2D) hydrodynamic model inundation extents at varying flood flows. The results from this analysis will help inform future restoration efforts by enhancing our understanding of carbon storage in relation to inundation dynamics.

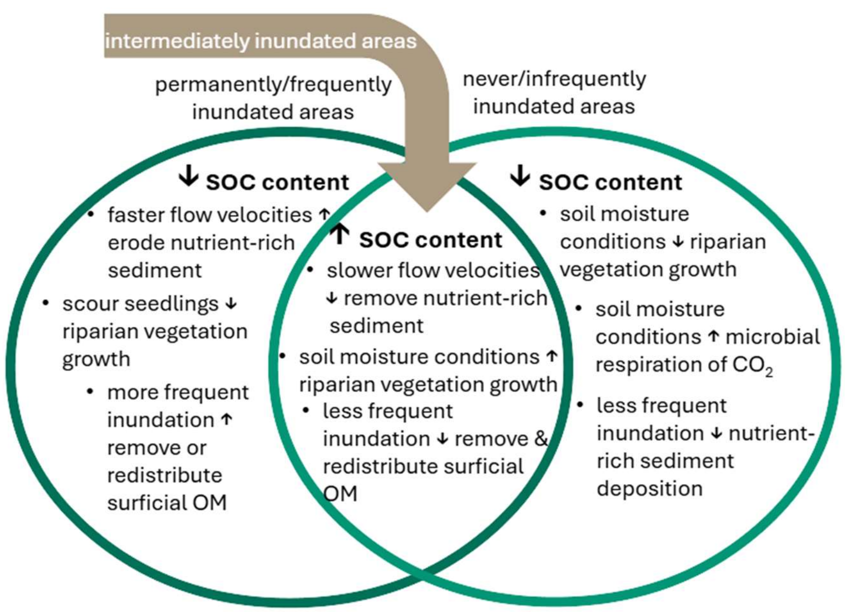

Figure 1. Conceptual model for intermediate inundation frequency hypothesis

2. METHODS

2.1 Study Area

I selected three floodplains located along Little Beaver Creek (LBC), Elkhorn Creek (LE), and the Laramie River (LRV) from a list of headwater streams slated for restoration by the Coalition for the Poudre River Watershed (CPRW). The floodplain locations are shown in Figure 2. CPRW's proposed restoration methods are low tech process-based restoration (LTPBR), which employs minimal machinery and relies on manual labor to install structures such as post-assisted log structures (PALS) or beaver dam analogs (BDAs) to increase channel-floodplain connectivity and capture burned hillslope fine sediments. I planned to collect all floodplain soil samples prior to structure installation. However, the final two days of sampling at LE coincided with structure installation.

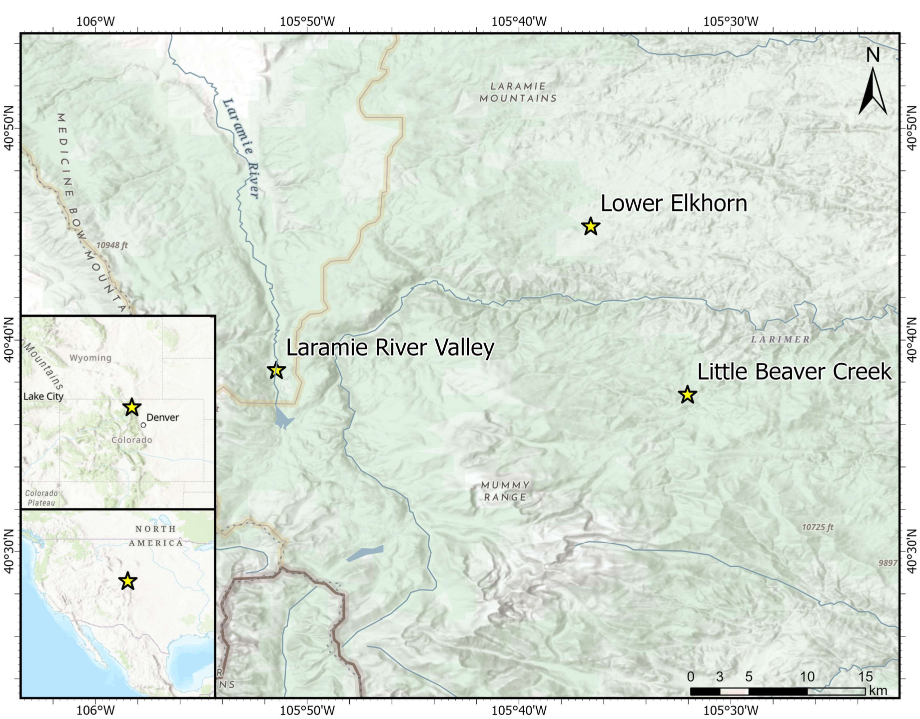

Figure 2. The three headwater stream floodplains of interest, located in the northern Colorado Rocky Mountains

2.1.1 Little Beaver Creek

LBC is located in northern Colorado's Rocky Mountains within the South Platte River Basin. LBC is a headwater tributary to the South Fork of the Cache La Poudre River with a drainage area of 47 km^2 (U.S. Geological Survey, 2019). The drainage area to the studied floodplain is 38 km^2 (U.S. Geological Survey, 2019). Additional geomorphic information is provided in Table 1. LBC's hydrograph is dominated by snowmelt peak flows in the late spring to summer and experiences flashy flows in the late summer due to convective thunderstorms. The LBC basin historically receives between 460 to 560 mm of precipitation annually (A. J. Hahn et al., 2025; Johnson et al., 1963). The LBC floodplain sits at an approximate elevation of 2,435 m.

The LBC floodplain is predominantly located on the left side of the channel with a steep and conifer-dominated slope (e.g., *Picea engelmannii*) on the right side of the channel (A. J. Hahn et al., 2025). The left side of the channel gradually slopes up towards a floodplain terrace and the vegetation transitions from willowy shrubs to grasses and sedges; a representative photo of the channel can be seen in Figure 3 and aerial imagery of the floodplain can be seen in Figure 4. The topography of the floodplain is generally continuous with few depressions or protrusions, except for a well-defined secondary channel that extends into the floodplain. Of the three reaches studied, there is limited evidence of historical beaver (*Castor canadensis*) activity along the modeled reach. The soils that make up the floodplain area are generally colluvium from the Precambrian igneous and metamorphic rocks that make up the northern Front Range mountains and gravelly alluvium/glaciofluvial deposits resulting from Cenozoic glacial activity (Chronic & Chronic, 1972; USDA Natural Resources Conservation Service, 2019; WECo, 2026). The breakdowns of sand, silt, and clay in the < 2 mm portion of the cores reserved for analyzing soil texture are provided in Table 4.

2.1.2 Lower Elkhorn

Elkhorn Creek is located in northern Colorado's Rocky Mountains within the South Platte River Basin. Elkhorn Creek is a headwater stream located near the Red Feather Lakes area and is tributary to the main fork of the Cache La Poudre River with a drainage area of 89 km^2 (U.S. Geological Survey, 2019). The floodplain of interest, LE, has a much smaller drainage area, 16 km^2, as it is near the source of the creek (U.S. Geological Survey, 2019). Like LBC and most headwater streams in Colorado, Elkhorn Creek's hydrograph is snowmelt dominated and experiences flashy flows in the late summer months due to convective storms. The Elkhorn Creek basin receives an average of 590 mm of precipitation annually (Christensen & Morrison, 2026). The LE floodplain sits at an approximate elevation of 2,625 m.

The LE floodplain is topographically and hydrologically complex. The channel is filled with roughness elements including large boulders, downed trees, and woody material that create backwater areas influencing the activation of side channels in the floodplain. A representative photo of the main channel is provided in Figure 3. In addition to surface water inputs, there are hummocks throughout the floodplain that fill with standing water, likely due to a shallow groundwater table, indicating that there may be a subsurface water input into the system. The shallow groundwater table likely influences vegetation growth, which supports the prolific growth of grasses (e.g., *Spartina pectinata*), sedges (e.g., *Carex spp.*), and shrubs (e.g., *Salix spp.*). Besides the depressions, relict beaver (*Castor canadensis*) berms were observed along the channel and spanning the floodplain, increasing the topographic heterogeneity. The soils that make up the floodplain area are primarily generated from granitic weathering (USDA Natural

Resources Conservation Service, 2019; WECo, 2026). The breakdown of sand, silt, and clay in the < 2 mm portion of the cores reserved for texture are provided in Table 4. Of the three floodplains, LE has the largest percentage of silt and clay sized particles.

2.1.3 Laramie River Valley

The Laramie River is located in northern Colorado's Rocky Mountains within the North Platte River Basin. The Laramie River is a headwater stream located near Cameron Pass and is tributary to the North Platte River with a drainage area of 11,189 km^2 (U.S. Geological Survey, 2019). The drainage area to the studied floodplain is 11 km^2 (U.S. Geological Survey, 2019). LRV experiences the same snowmelt dominated hydrograph as LBC and LE. The LRV basin historically receives between 798 and 1,636 mm of precipitation annually (USDA Natural Resources Conservation Service, 2026). The precipitation data were collected at the Joe Wright snow telemetry station, located within a 16 km radius of the LRV floodplain. The LRV floodplain sits at an approximate elevation of 2,675 m.

The LRV floodplain is predominantly located on the left side of the river. To the right of the channel is a steeply sloped scree field. The floodplain supports an abundant willow (e.g., *Salix* spp.) population. The channel has incised significantly along the middle portion of the modeled reach, and the banks were actively sloughing during field data collection. I found evidence of many relict beaver (*Castor canadensis*) berms along with the presence of two active dams and their associated ponds (Figure 3). The floodplain itself is crossed by multiple secondary channels that become more densely vegetated as the distance from the channel increases. The slopes surrounding the floodplain were burned during the 2020 Cameron Peak fire; however, the trees located on the floodplain suffered less damage. The soils that make up the floodplain area are generally alluvium from the Precambrian igneous and metamorphic rocks that make up the northern Front Range mountains and gravelly alluvium/glaciofluvial deposits resulting from the Cenozoic glacial activity (Chronic & Chronic, 1972; USDA Natural Resources Conservation Service, 2019; WECo, 2026). The breakdown of sand, silt, and clay in the < 2 mm portion of the cores reserved for texture are provided in Table 4. Of the three floodplains, LRV has the largest percentage of sand-sized particles.

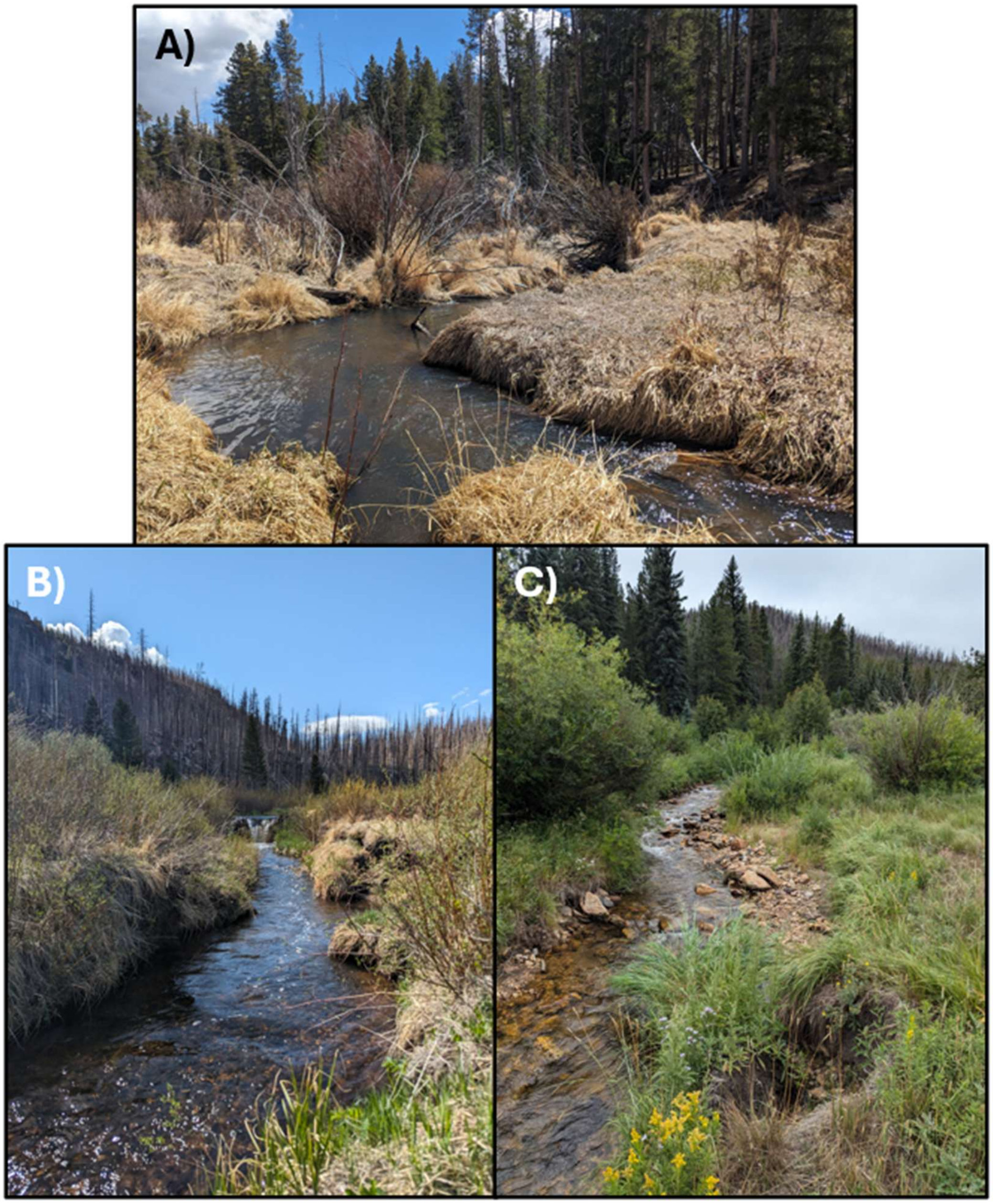

Figure 3. Representative photos from all three sampled floodplain rivers, LE (Panel A), LRV (Panel B), and LBC (Panel C)

Table 1. Select floodplain geomorphic parameters for all sampled floodplains

Geomorphic Parameters	LBC	LRV	LE
Slope (m/m)	0.026	0.011	0.023
Sinuosity	1.27	1.41	1.35
Average bankfull depth (m)	1.11	0.85	0.94
Modeled watershed area (km^2) (U.S. Geological Survey, 2019)	37.55	10.57	16.19
Modeled Reach length (m)	594	929	285
Floodplain elevation (m ASL)	2,435	2,625	2,675

2.2 Field Data Collection

I conducted field data collection over two summers: LBC in 2024 and LRV and LE in 2025.

2.2.1 Topographic Surveys

I collected a bathymetric survey for the reach of interest to use in hydrodynamic modeling. I used RS2 and RS3 EMLID real-time kinematic global navigation satellite system (RTK GNSS) receivers to capture the channel survey data. At each floodplain, control points were identified and were surveyed at the beginning of each survey workday. In addition to the control points, I collected road survey shots to help adjust the bathymetric survey to existing LiDAR. The elevation of the road is static compared to the dynamic nature of channel bed and banks, thus providing a reference to vertically correct the bathymetric survey.

To survey the channel, I collected survey points approximately 10 cm apart spanning a cross-section perpendicular to the channel, toe of bank to toe of bank. I spaced the cross-sections longitudinally, based on the complexity of the channel. For example, relatively homogeneous stretches of channel were surveyed at the beginning and ending of the section, while complex bedforms were surveyed more intensely to accurately capture variability that could influence model flow characteristics. I collected bathymetric surveys for LRV and a portion of LE at the beginning of the 2025 field season. I was able to use previously collected bathymetric survey data for LBC and portions of LE (Christensen, 2025).

In addition to the bathymetric survey, the hydrodynamic model requires flow measurements paired with a water surface elevation (WSEL) survey. These data are used to calibrate and validate the model. I collected two discharge measurements using a SonTek FlowTracker2 Handheld-ADV at the upstream end of the LRV reach. These data were collected on the same day as a WSEL survey, which was collected using an RS2 RTK GNSS receiver and base station. Paired WSEL and discharge data were collected previously for LBC and LE.

2.2.2 Core Collection

To prepare for field data collection, I created relative elevation maps (REMs) of each floodplain from light detection and ranging (LiDAR) flown in 2020 (CWCB, 2020). The REMs were broken up into six elevation bins, 0.0-0.25, 0.25-0.5, 0.5-0.75, 0.75-1.0, 1.0-1.25, and >1.25 m above the channel. I drew transects perpendicular to the channel and randomly selected points, ensuring there were eight coring locations in each elevation bin for LBC and nine for LE and LRV. I uploaded the REMs and proposed coring locations to an iPad in the Avenza app. Due to geospatial uncertainty in the field, proposed core elevation bins were not always consistent with actual core elevation bins. Core relative surface elevations to the channel were extracted from the REMs in a geographic information system (ArcGIS Pro 3.3.0, ESRI, Redlands, CA, USA) (hereafter referred to as ArcGIS) following sample collection. Cores that were corrected following field work are provided in Appendix A: Applicable Lab and Field Information. Figure 4 shows the location of all cores and their final relative surface elevation above the channel.

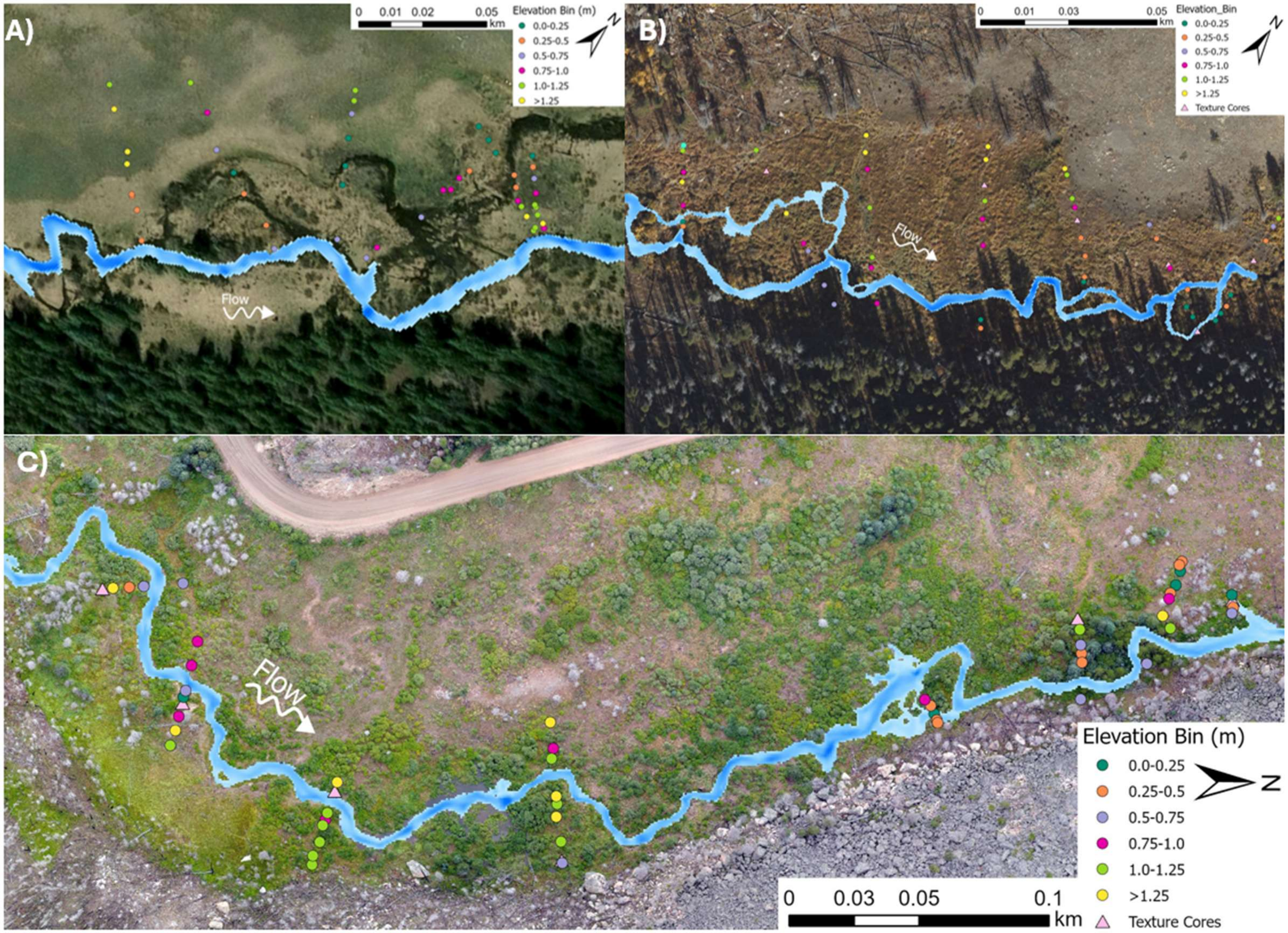

Figure 4. LBC floodplain aerial imagery with soil core locations depicted and their respective relative elevation bins (Panel A). LE floodplain aerial imagery with soil core locations depicted and their respective relative elevation bins (Panel B). LRV floodplain aerial imagery with soil core locations depicted and their respective relative elevation bins (Panel C).

I collected floodplain soil cores from LBC in July and August 2024 and I collected floodplain soil cores from LE and LRV in June and July 2025. The in-field sample collection spanned multiple days for each floodplain. To collect a sample, I navigated to the proposed soil core location and marked the geospatial location in the Avenza app. At each proposed location, I collected an organic layer sample and multiple mineral samples. The organic layer sample consisted of the surficial litter and duff as well as the root-bound soil layer within a rectangular area. I measured and recorded the dimensions of the rectangle to calculate its bulk density (Lininger et al., 2019). Once the organic layer sample was collected, mineral sample collection began. I utilized an AMS soil corer that had a length of 18 cm and an opening diameter of 5.08 cm. I collected mineral samples in 18 cm increments (see Figure 5 for an example core), recording total depth following each extraction, until 1 m in depth was reached or core extraction was no longer possible (Lininger et al., 2019). I encountered two scenarios in the field that halted core collection: soil saturation at which the soil could not be removed, and the presence of coarse alluvium or large rocks that could not be cored through. I qualitatively described each organic and mineral layer sample in the field. An example of the field notes taken for a core can be found in Appendix A:

Figure 5. Soil core example

2.3 Laboratory Processing

Following field collection, samples were frozen until processing began. I stored and processed all samples at the U.S. Forest Service Rocky Mountain Research Station (RMRS).

2.3.1 Mineral Samples

To process the floodplain soil cores, I dried the samples, either through air drying or a combination of air drying and a 60 ˚C oven, until they were able to be dry sieved. I recorded the weight of the wet and dry sample and then transferred the sample into a mortar and pestle to break up the prevalent soil aggregates. These soil aggregates are either formed through inorganic binding agents or organo-mineral association (Tisdall & Oades, 1982). These aggregates can physically shield SOC and fine OM from microbial decomposition (Sufian, 2021). Throughout the mortar and pestling process, I continuously sieved the sample using a 2 mm mesh sieve until all the <2 mm particles were separated (ASTM Test Sieve, No. 10). I used this sieve to remove organic material and allow sand size particles and smaller to pass through, as most organic carbon adsorbs to these particles (Appling et al., 2014; Hassink & Whitmore, 1997; Sutfin &

Wohl, 2017). I recorded the mass of both the >2 and <2 mm portion of the samples and then measured out 10 g of the <2 mm portion. I dried each 10 g sample at 60 ˚C for >24 hours to ensure the sample was completely dry and recorded this final weight. I then transferred the 10 g samples into 200 mL scintillation vials. Into each scintillation vial I added 10-15 metal beads. The scintillation vials were placed in a large Nalgene and filled with mesh to ensure the vials stayed in place. I placed the Nalgenes on a long roll jar mill and allowed them to roll for at least 72 hours; certain samples remained on the mill longer due to the persistence of large particles.

To isolate the organic carbon fraction present in the floodplain soils, I selected random samples (LBC n = 15, LRV n = 10, and LE n = 10), without knowing the location, depth increment, or elevation bin, from each floodplain to perform an inorganic carbon test. I weighed out a >100 mg subsample into plastic weigh boats. I then applied three drops of a 2 M HCl solution to each. I watched and listened for the presence of effervescence and allowed the samples to dry for an hour. I applied three more drops of the HCl solution and again observed for effervescence (ISO, 1995). I dried the HCl treated samples completely either using a 60 ˚C oven or at room temperature prior to their elemental analysis. This process was completed prior to running all of the mineral samples on the elemental analyzer (EA), VELP-CN802. The VELP outputs total carbon, which includes both the inorganic and organic carbon present in the soil sample.

I prepared each mineral sample for the VELP by measuring ~100 mg of sample into a square of tin foil. I input the weight of each subsample into the VELP software in conjunction with the sample. I performed the same process on the inorganic samples; their weight varied from 100 mg depending on the amount initially treated with HCl. The instrument computed the amount of carbon present in each sample in mgs, and weight-based percent carbon. I subtracted the percent carbon computed by the VELP for the acidified samples from the total carbon measured in the untreated samples. Due to the small amount of inorganic carbon present in the tested samples (0.0-0.8%, 0.0-0.2%, and 0.0-0.7% for LBC, LRV, and LE, respectively), I assumed the total carbon measured by the EA analysis to be organic carbon.

I used the data collected during sample processing to determine each sample's bulk density (BD), total and hybrid (<2 mm), see Eq. (1) and (2), respectively. To determine the total BD, I calculated the dry mass of each sample. As explained earlier, certain samples were dried at 60 ˚C before they were sieved. Due to differences in drying, I multiplied the relative change before and after drying the 10 g sample by either the initial <2 mm portion of the sample or the dried <2 mm portion of the sample. To the corrected <2 mm values, I added the mass of the coarse portion (>2 mm) of the sample. I then divided the resultant sum by the volume of the cylindrical core, using the radius of the corer and the length of the core (measured as depth in the field), to get each sample's total BD (Lininger & Polvi, 2020). The calculation is the same for the hybrid BD, except the coarse sediment mass is excluded (Lang et al., 2025). The hybrid BD corrects for the presence of root and rock volume throughout the floodplain, reducing the chance of overestimating SOC stock (Lang et al., 2025; Reed et al., 2022; Throop et al., 2012). I calculated both BDs to allow for comparison with past literature, which commonly reported SOC stock using total BD (Throop et al., 2012).

$$\text{Total BD}\left(\frac{g}{cm^3}\right) = \frac{\left(<2\text{ mm dry bulk mass} * \frac{(10\text{g wet mass} - 10\text{g dry mass})}{10\text{g dry mass}}\right) + (>2\text{ mm soil mass})\ (g)}{\text{Core Volume (cm}^3\text{)}} \tag{1}$$

$$\text{Hybrid BD}\left(\frac{g}{cm^3}\right) = \frac{\left(<2\text{ mm dry bulk mass} * \frac{(10\text{g wet mass} - 10\text{g dry mass})}{10\text{g dry mass}}\right)\ (g)}{\text{Core Volume (cm}^3\text{)}} \tag{2}$$

To calculate SOC stock for the active layer or depth sampled, I used Eq. (3) (Lininger et al., 2019). Each mineral sample's OC stock was calculated and all samples were summed to determine the total amount of OC stock per core location. Many papers extrapolate from the active layer to 1-m in depth (Hinshaw & Wohl, 2023; Lininger et al., 2019). Eq (4) provides the calculation to determine the OC stock for each floodplain down to a meter in depth.

$$\text{Active Layer OC Stock } \left(\frac{Mg\ C}{ha}\right) = \sum OC\ (\%) * Hybrid\ BD\ \left(\frac{g}{cm^3}\right) * Depth\ of\ scample\ increment(cm) * 100 \qquad (3)$$

$$\text{1-m OC Stock } \left(\frac{Mg\ C}{ha}\right) = Avg. Mineral\ Core\ OC\ (\%) * Avg. Mineral\ Core\ Fine\ BD\ \left(\frac{Mg}{m^3}\right) * 1\ m * 10{,}000\ \frac{m^2}{ha} \qquad (4)$$

2.3.2 Grain Size Analysis

To characterize the soil texture of LE and LRV, I assessed sample-level soil texture on a subset of samples (n = 6) from each site and depth using the hydrometer method adapted from Milford (2010), with measurements performed using a standard hydrometer (Taylor Scientific, St. Louis, MO).

I separated out the fine sediment fraction from the texture samples using the same process described previously. I then weighed out 50 g of the sample into a stainless steel mixing cup, added 2.0 grams of sodium metaphosphate to break up any remaining soil aggregates, and filled the stainless steel mixing cup with water until it was two-thirds full. I placed the stainless steel mixing cups on a triple spindle drink mixer that stirred the samples for 5 minutes. I transferred the soil-water mixture to settling cylinders and collected two hydrometer and temperature readings. I recorded the first set of hydrometer and temperature readings 40 seconds after the cylinders were agitated. I then collected the second set of hydrometer and temperature readings after 6 undisturbed hours.

The LBC texture samples were collected by collaborators at RMRS. I assisted in processing the LBC texture samples using the same laboratory methodology; however, the LBC samples needed to be combined to reach a mass of 50 g as the corer used was smaller in diameter and length. The samples were combined based on texture, depth, and geomorphic unit similarity.

To determine the percent sand, silt, and clay for each sample, I corrected the hydrometer reading depending on whether the mixture temperature was above or below 20 ˚C; see Eq. (5) and (6), respectively. Following the correction, I calculated the percent clay, Eq. (7), percent silt, Eq. (8), and percent sand, Eq. (9) (Gee & Bauder, 1986; Milford, 2010).

$$\text{Corrected Hydrometer Reading} = \text{Hydrometer Reading}\left(\frac{g}{L}\right) + \left[(\text{Temp. (°C)} - 20) * 0.36\left(\frac{g}{L}\right)\right] \tag{5}$$

$$\text{Corrected Hydrometer Reading} = \text{Hydrometer Reading}\left(\frac{g}{L}\right) - \left[\left(20 - \text{Temp. (°C)}\right) * 0.36\left(\frac{g}{L}\right)\right] \tag{6}$$

$$\%\ \text{clay} = \frac{\text{Corrected 6-hour hydrometer reading} * 100}{\text{Oven-dry weight of soil}} \tag{7}$$

$$\%\ \text{silt} = \frac{\text{Corrected 40-second hydrometer reading} * 100}{\text{Oven-dry weight of soil}} - \%\ \text{clay} \tag{8}$$

$$\%\ \text{sand} = 100 - (\%\ \text{silt} + \%\ \text{clay}) \tag{9}$$

2.3.3 Organic Samples

To determine the amount of carbon in the organic samples, I used a weight loss on ignition (LOI) method. I first weighed the organic layer sample prior to drying. I then dried each sample in a 60 ˚C oven for 48-72 hours, at which point the samples were reweighed. I then returned the samples to the oven for another 24 hours and remeasured their weights. After each weight measurement, I calculated a percentage difference between drying periods. Once the percentage difference was smaller than 1%, I removed the samples and placed them in a cool dry area until incineration could be completed.

To incinerate the samples, I placed each in a ceramic crucible with the sample name written in graphite. I recorded the weight of the crucible and the weight of the sample before and after incineration. To reduce the chances of losing sample in the aerated oven, I placed tin foil over the majority of the crucible. While preparing the sample, I heated the oven to 450 ˚C and then placed 5-6 samples into the oven. I started a 4-hour timer once the oven reached 450 ˚C. At the end of the 4 hours, the samples were removed promptly and placed on ceramic stands to cool (Cambardella et al., 2000). The weight loss from ignition was measured and converted into percent carbon using a conversion factor of 0.58, which assumes that 58% of OM is carbon (De Vos et al., 2005; Lininger et al., 2018; Pribyl, 2010).

In collaboration with the RMRS, I milled twenty samples, ten from LE and ten from LRV, to analyze a subsample of the organic layer on the VELP. The RMRS collected organic and mineral layer samples at LBC; to better compare our results, they also processed a subset of their organic layer samples using an LOI method. We took these actions to determine whether the methodologies chosen would be conducive for organic layer carbon content comparison.

2.4 Hydrodynamic Model Development

To determine the extent of inundation at each floodplain, I created two hydrodynamic models in Sediment and River Hydraulics-two dimension (SRH-2D), one for the 929 m LRV reach and one for the 285 m LE reach. For LBC, I was able to utilize a pre-existing SRH-2D model of the 594 m reach (Christensen, 2025). The SRH-2D software uses the depth-averaged St. Venant Equations to predict variables such as water surface elevation, depth, and depth-averaged velocity (Bureau of Reclamation, 2024). I chose to model the two reaches in the SRH-2D application due to previous model development as well as the implementation of the obstruction feature to model the two active beaver dams at LRV.

2.4.1 Terrain Development

Creating a hydrodynamic model in SRH-2D requires a topographic surface of the modeled reach. To create the LRV and LE surfaces, respectively, I leveraged 1 ft x 1 ft (0.305 m x 0.305 m) resolution LiDAR flown by Ayers Associates in 2024 and 2025. The interaction of water and the wavelength used in LiDAR inhibits the capture of channel bedform topographic variability. Therefore, I used the field-collected bathymetric survey data to characterize the channel bed surface. I corrected the surveyed bathymetry data laterally using a Continuously Operating References Station for LRV and the Online Positioning User Service correction for LE (National Geodetic Survey, 2025a, 2025b). I corrected both floodplains vertically using road survey shots. Once the channel survey points were corrected, I imported these into ArcGIS, where I created a triangular irregular network (TIN) of the channel using the "Create TIN" tool in ArcGIS. I manipulated the TIN node connections to connect upstream and downstream points. The LiDAR was shared as a digital elevation model (DEM) file, which is a type of Raster. To merge the bathymetric surface and the terrestrial surface, I converted the TIN to a raster using the "TIN to Raster" tool. I then merged the two Rasters and imported the updated surface file into SRH-2D.

2.4.2 Model Characteristics

Two boundary conditions (BC) need to be specified in an SRH-2D model; one at the upstream end of the modeled reach and one at the downstream end. I observed subcritical flow characteristics at the upstream and downstream extents of the model at both LRV and LE. Therefore, I opted to use the "Inlet-Q (subcritical inflow)' BC and "Exit-H (subcritical outflow)" BC.

For the upstream BC, I input the various flows as a time series that ramped from zero to the desired flow over one hour for LE and one and a half hours for LRV. I selected the time series option over the constant flow option due to water pooling on the floodplain incongruous with reality. I lengthened the inlet flow ramp up for the 10-, 25-, and 50-yr for LRV and the 500-yr for LE. The model had greater stability associated with the longer ramp up period for these flows. Each simulation ran for a minimum of five hours, ensuring steady state was reached.

For the downstream BC, I computed an estimated WSEL using the integrated Channel Calculator feature. The calculator required a ground elevation dataset, composite Manning's n, reach slope, and the minimum and maximum flows. I calculated the slope of the channel using measurement tools in ArcGIS in conjunction with the highest and lowest thalweg elevations. All but the composite Manning's n value remained constant for the modeled flows. I updated the composite Manning's n depending on the amount of floodplain activation for the associated discharge.

In addition to BCs, SRH-2D requires the creation of a surface mesh. The mesh pulled elevation data from my combined surface raster, allowing the model to incorporate the topographic variation in its calculations. I specified the mesh type for both the floodplain and channel areas as a paving or triangular mesh (LRV: 52,186 nodes and 104,135 elements; LE: 11,472 nodes and 22,794 elements). The triangular mesh element distribution ranged in length between 1 to 10 m for LRV and 0.75 to 5 m for LE, with the triangular element size increasing with distance from the channel. I attempted smaller mesh sizes for LRV, but the smaller mesh sizes resulted in simulation failure even with adjustments to the inlet BC flow and model time step.

An additional SRH-2D component was added to the LRV model due to the presence of two beaver dams and their subsequent ponds. I used the obstruction feature along with an area of increased roughness to represent the beaver dams. The obstruction feature required inputs for width, bottom elevation, depth, drag coefficient, and porosity. The values used for both dams, upstream (US) and downstream (DS), are provided in Table 2. I calculated the width of both dams using aerial imagery flown by Ayers Associates in 2025 and measurement tools in ArcGIS. For the bottom elevation and depth, I cut cross-sections across the merged LiDAR and bathymetric surface to determine the thalweg elevation as well as the depth measurement from top of bank to the bottom of the channel. The drag coefficient and porosity were assigned based on previous studies and the fact that decreasing the porosity negated the effects of the obstruction (Aquaveo Staff, 2022; Schultz et al., 2025). The backwatering effect of the obstruction features did not achieve the WSELs recorded in the field. Using the aerial imagery, I delineated each dam area and updated this area's roughness coefficient which marginally improved the WSEL accuracy behind the dam.

Table 2. Beaver dam obstruction inputs

Beaver dam	Width (m)	Bottom elevation (m)	Depth (m)	Drag coefficient	Porosity
US	1.82	2667.81	1.66	1.0	0.1
DS	3.11	2665.94	0.94	1.0	0.1

2.4.3 Model Calibration and Validation

Two important inputs into the SRH-2D model are the Manning' *n* values for the channel and floodplain, which are empirical coefficients that represent a surface's hydraulic roughness. Commonly, the channel roughness factor is updated iteratively to improve the performance of a hydraulic model, but there are methods that have been developed to systematically estimate an initial *n* value for both the channel and the floodplain (Aldridge & Garrett, 1973; Arcement & Schneider, 1989; Limerinos, 1970). I estimated my initial channel and floodplain *n* values using the modified Cowan (1956) procedure combined with in-field observations (Arcement & Schneider, 1989). The estimations resulted in channel *n* values of 0.098 and 0.075 and floodplain *n* values of 0.21 and 0.16 for LRV and LE, respectively. More detailed information on the calculation and justification of the initial values is included in Appendix B: Manning's *n* Calibration and Validation. I calibrated the LRV and LE models using coupled discharge and

WSEL data collected on June 5th, 2025, and May 16th, 2024, respectively. I collected an additional set of discharge and WSEL data for validation of the model on May 30th, 2025, and June 3rd, 2024, for LRV and LE, respectively. I used the largest measured discharge to calibrate the model and the smaller was used for validation. To calibrate the model, I modified the initial channel *n* value iteratively to calculate the most accurate WSELs (i.e., lowering the model's root mean square error (RMSE)) along the modeled reach for the calibration flow. The calibrated channel Manning's *n* values were validated using the paired validation data. The calibration and validation discharges and their finalized modeled statistics, mean error (ME) and RMSE, are provided in Table 8. Detailed documentation of the calibration process is included in Appendix B: Manning's *n* Calibration and Validation.

2.4.4 Model Simulations

To determine which cores were inundated during a flood event, I modeled a range of recurrence interval flows. I leveraged the USGS StreamStats software to estimate the 2-, 5-, 10-, 25-, 50-, 100-, 200-, and 500-year recurrence interval discharges for each floodplain (U.S. Geological Survey, 2019). Steady-state simulations were run for each flood simulation. Each floodplain's recurrence interval flow rates (Q) are presented in

Table 3.

Table 3. Each floodplain’s recurrence interval discharges (U.S. Geological Survey, 2019)

Recurrence interval	LBC Q (cms)	LRV Q (cms)	LE Q (cms)
2-year	1.83	1.74	0.98
5-year	2.83	2.46	1.52
10-year	3.6	2.92	1.93
25-year	4.5	3.51	2.41
50-year	5.55	4.16	2.94
100-year	6.4	4.62	3.43
200-year	7.16	4.98	3.82
500-year	8.66	5.80	4.59

2.5 Statistical Analysis

To determine if there were statistically significant differences in SOC between the sampled relative elevation bins and cores grouped by inundation, I conducted three statistical tests in R (version 4.5.2) using base functions. These tests were performed on the full sample and mineral-only sample sets for each floodplain. The first test, the Shapiro-Wilk test, is used to determine whether the data have a normal distribution (Shapiro & Wilk, 1965). The Shapiro-Wilk test showed that the elevation bin data consistently deviated from normality for LBC, LRV, and LE. In addition to the Shapiro-Wilk test, I created a qq-plot for each floodplain to visually confirm the Shapiro-Wilk test, which showed that when considering the entire dataset for each floodplain, the data were not normally distributed. The qq-plots are provided in Appendix C: Statistical Normality Data.

Since the data lacked normality, I performed a non-parametric Kruskal-Wallis test to determine if the amounts of carbon between elevation bins and cores grouped by initial inundation discharge were significantly different (Kruskal & Wallis, 1952). On the data sets that showed statistical differences, I conducted a pairwise Wilcoxon rank sum test to obtain the exact groups that had statistically significant differences. The Wilcoxon rank sum test p-values were adjusted using the Benjamini-Hochberg procedure to reduce the chance of false positives or type I errors (Benjamini & Hochberg, 1995; Wilcoxon, 1945).

3. RESULTS

3.1 Floodplain SOC Content

Forty-eight cores were collected from each floodplain for EA and an additional eight were collected at LRV and LE for texture analysis. Table 4 presents the texture and bulk density data and Table 5 presents the distribution of cores in each elevation bin per floodplain. Each floodplain had varying amounts of SOC present with the mean and standard error (SE) for percent carbon being 8.19% ± 0.51 for LBC (median = 5.85%), 4.05% ± 0.28 for LRV (median = 2.72%), and 6.80% ± 0.41 for LE (median = 5.23%). All SOC values decreased for the mineral-only dataset, resulting in mean and SE for percent carbon values of 5.06% ±0.34 for LBC (median = 4.02%), 2.36% ± 0.12 for LRV (median = 1.92%), and 4.99% ± 0.36 for LE (median = 3.88%). LBC had the highest mean SOC among the three floodplains.

Table 4. Floodplain specific field and lab results

	LBC	**LRV**	**LE**
Number of cores | Total number of samples	48 | 166	54 | 261	54 | 211
Organic	46	54	54
Mineral	120	207	157
Number of cores | Number of texture samples	NA	6 | 23	6 | 15
Percent Silt (%)	32.66	25.36	30.96
Percent Clay (%)	7.82	12.71	21.79
Percent Sand (%)	59.53	61.93	47.25
Average Total Bulk Density (g/cm^3)	0.67 ± 0.035	0.96 ± 0.045	0.92 ± 0.14
Average Hybrid Bulk Density (g/cm^3)	0.71 ± 0.025	0.99 ± 0.039	1.04 ± 0.18

Table 5. Distribution of cores per elevation bin for all floodplains

Elevation Bin (m)	LBC		LRV		LE	
	No. of cores	No. of mineral samples	No. of cores*	No. of mineral samples*	No. of cores*	No. of mineral samples*
0.0-0.25	8	16	5	12	8	18
0.25-0.5	10	25	10	28	9	23
0.5-0.75	7	22	8	36	5	15
0.75-1.0	8	14	7	23	10	26
1.0-1.25	10	25	11	53	8	32
>1.25	5	18	7	32	8	28
Total	48	120	48	184	48	142

*Not including cores or samples reserved for textural analysis

3.1.1 Floodplain SOC Compared to Relative Elevation Above the Channel

Figure 6 compares the depth-averaged percent carbon, which excludes the organic layer, against each core's relative surface elevation. For the LBC and LRV floodplains there appears to be a negative correlation between carbon content and relative surface elevation above the channel. When considering LE, we see a positive correlation for the same comparison. For all three floodplains the coefficient of determination, R^2, is quite low (0.26, 0.08, and 0.02) and only one of the p-values rejects the null hypothesis (LBC = 1.97e-4). I produced linear regressions for the volume-averaged percent carbon, which includes the organic layer (included in Appendix D: Relationship between Volume Averaged Percent Carbon and Relative Surface Elevation Above the Channel). Those linear regressions followed the same pattern; negative for LBC and LRV and positive for LE. Although the relationships hold, the prediction ability and strength both decrease when the organic samples are included.

Table 6 provides summary statistics for the depth-averaged percent carbon for all three floodplains broken into entire floodplain categories and relative elevation bins.

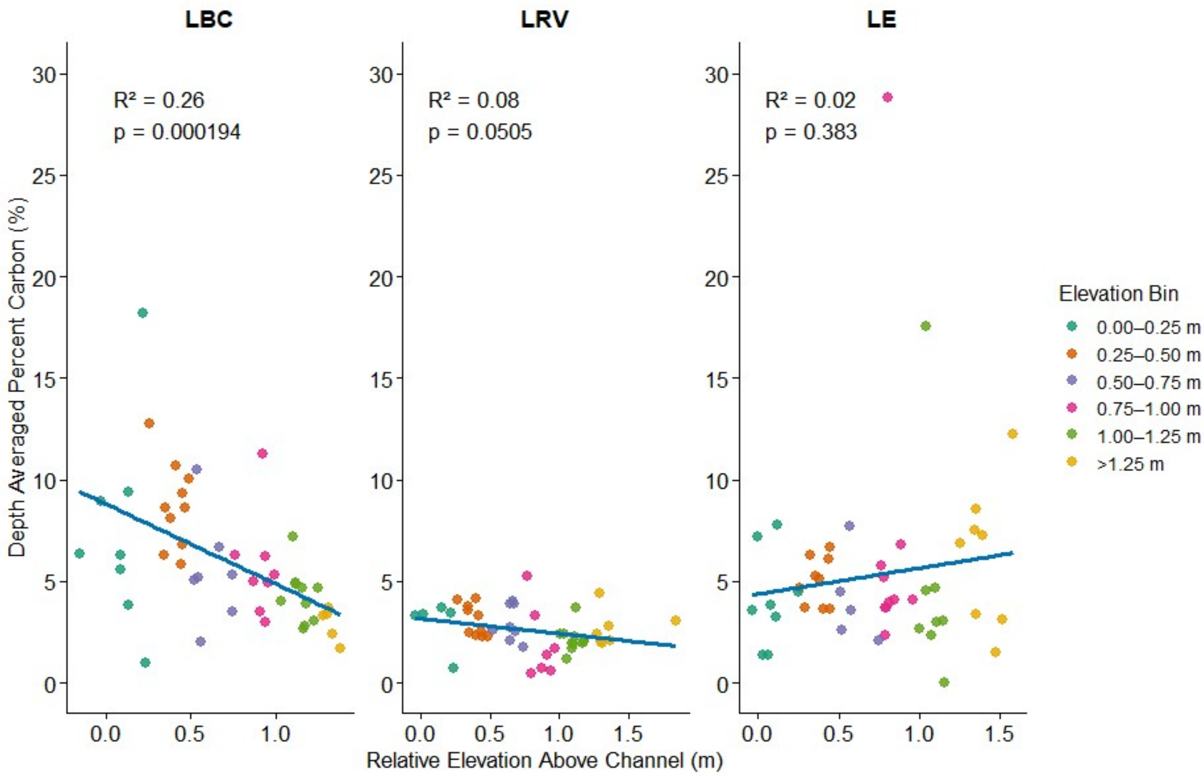

Figure 6. Depth-averaged percent carbon against relative surface elevation above the channel for the LBC, LRV, and LE floodplains

Table 6. Depth-averaged percent carbon summary statistics

		Entire	0.00-0.25	0.25-0.5	0.5-0.75	0.75-1.0	1.0-1.25	>1.25
		% C	% C	% C	% C	% C	% C	% C
Min.	LBC	0.96	0.96	5.81	2.04	2.98	2.66	1.68
	LRV	0.44	0.74	2.25	1.74	0.44	1.17	1.94
	LE	0.00	1.35	3.63	2.09	2.36	0.00	1.48
Max.	LBC	18.21	18.21	12.76	10.49	11.30	7.18	3.69
	LRV	5.26	3.72	4.18	4.01	5.26	3.68	4.42
	LE	28.77	7.80	6.68	7.70	28.77	17.52	12.26
Median	LBC	5.23	6.31	8.61	5.17	5.16	4.35	3.33
	LRV	2.41	3.39	2.94	2.65	1.40	2.03	2.39
	LE	4.09	3.70	5.14	3.59	4.09	3.01	7.06
Mean	LBC	5.99	7.44	8.70	5.48	5.68	4.27	2.89
	LRV	2.60	2.93	3.08	2.93	1.92	2.14	2.68
	LE	5.31	4.10	5.02	4.10	6.84	4.72	6.30
Std. Dev.	LBC	3.27	5.12	2.13	2.66	2.55	1.34	0.83
	LRV	1.07	1.23	0.78	0.88	1.76	0.62	0.88
	LE	4.52	2.37	1.19	2.22	7.81	5.37	3.49

The results from the Kruskal-Wallis tests showed that the depth-averaged percent carbon differed significantly for LBC ($\chi^2 = 21.86$, df = 5, p = 5.57e-4) and LRV ($\chi^2 = 11.939$, df = 5, p = 3.56e-2). There was no statistically significant difference between any elevation bins for the LE dataset. The adjusted p-values from the Wilcoxon rank sum test for the LE and LRV datasets are provided in

Table 7 with the statistically significant different p-values in bold font. Soil core profiles from each elevation bin were grouped and plotted for the bins that were found to have statistically significant differences. Figure 7 provides the 0.25-0.5 m and 1.0-1.25 m elevation bin cores at LRV with individual percent carbon values for each sample as well as depth-averaged percent carbon values for the entire core depicted. Figure 8 provides the same information, but for the 0.25-0.5 m (bordered in orange to highlight its comparison with the other three elevation bins provided), 0.75-1.0 m, 1.0-1.25 m, and >1.25 m elevation bins at LBC.

Table 7. Pairwise-Wilcoxon rank sum test results (bolded adjusted p-values values indicate elevation bins with statistically significant differences)

	LBC	**LRV**
Elevation Bin Comparison	p-values	p-values
0.0-0.25 vs 0.25-0.5	0.3215	1.000
0.0-0.25 vs. 0.5-0.75	0.4252	1.000
0.0-0.25 vs. 0.75-1.0	0.3215	0.337
0.0-0.25 vs. 1.0-1.25	0.1386	0.336
0.0-0.25 vs >1.25	0.0738	0.46
0.25-0.5 vs. 0.5-0.75	0.0509	1.000
0.25-0.5 vs. 0.75-1.0	**0.0427**	0.277
0.25-0.5 vs. 1.0-1.25	**0.0011**	**0.041**
0.25-0.5 vs. >1.25	**0.0050**	0.405
0.5-0.75 vs. 1.75-1.0	0.9551	0.336
0.5-0.75 vs. 1.0-1.25	0.2635	0.153
0.5-0.75 vs. >1.25	0.1028	0.766
0.75-1.0 vs. 1.0-1.25	0.1517	0.336
0.75-1.0 vs. >1.25	0.0559	0.336
1.0-1.25 vs. >1.25	0.103	0.336

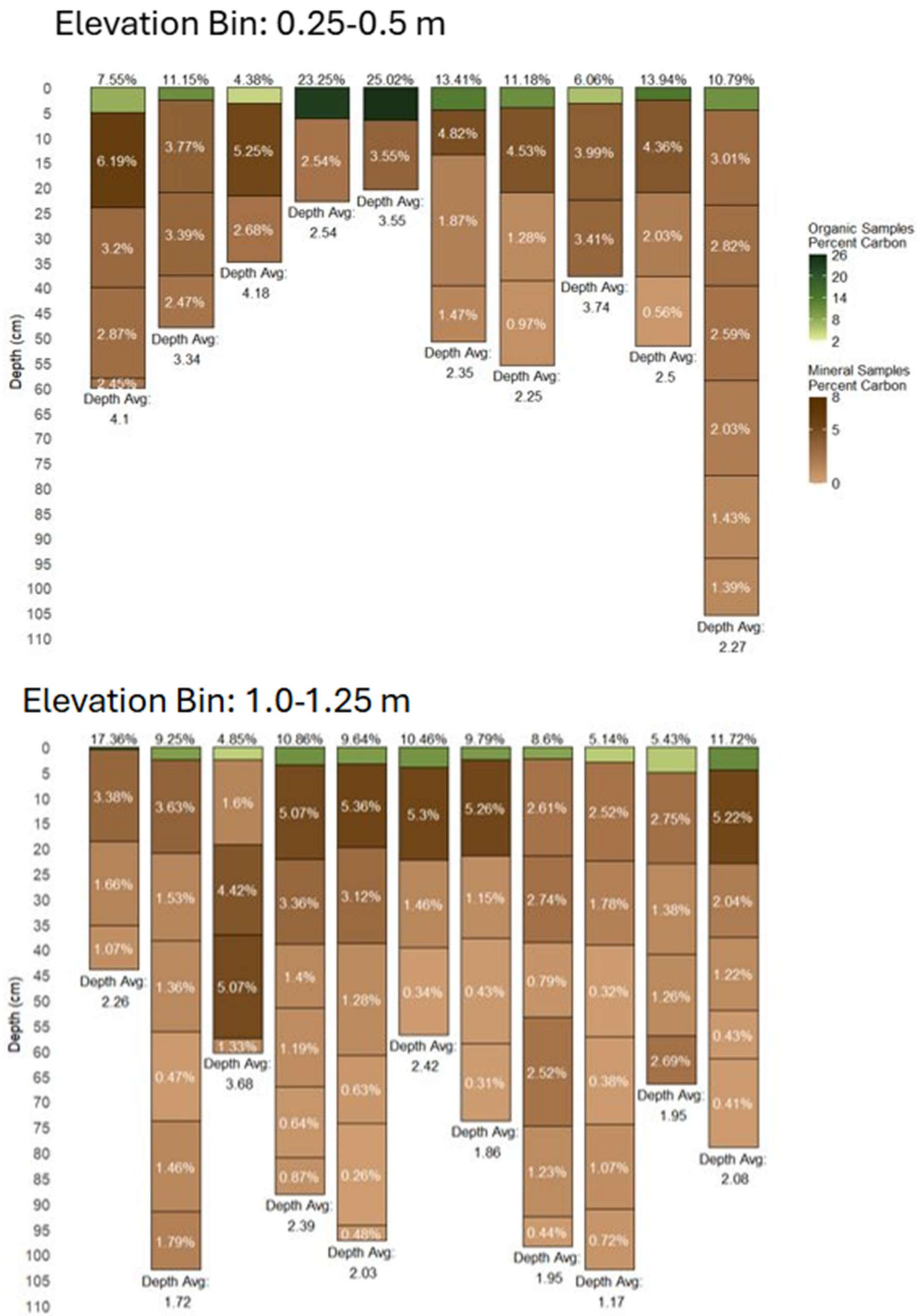

Figure 7. LRV soil core profiles for elevation bins with significant differences (0.25-0.5 vs. 1.0-1.25 m)

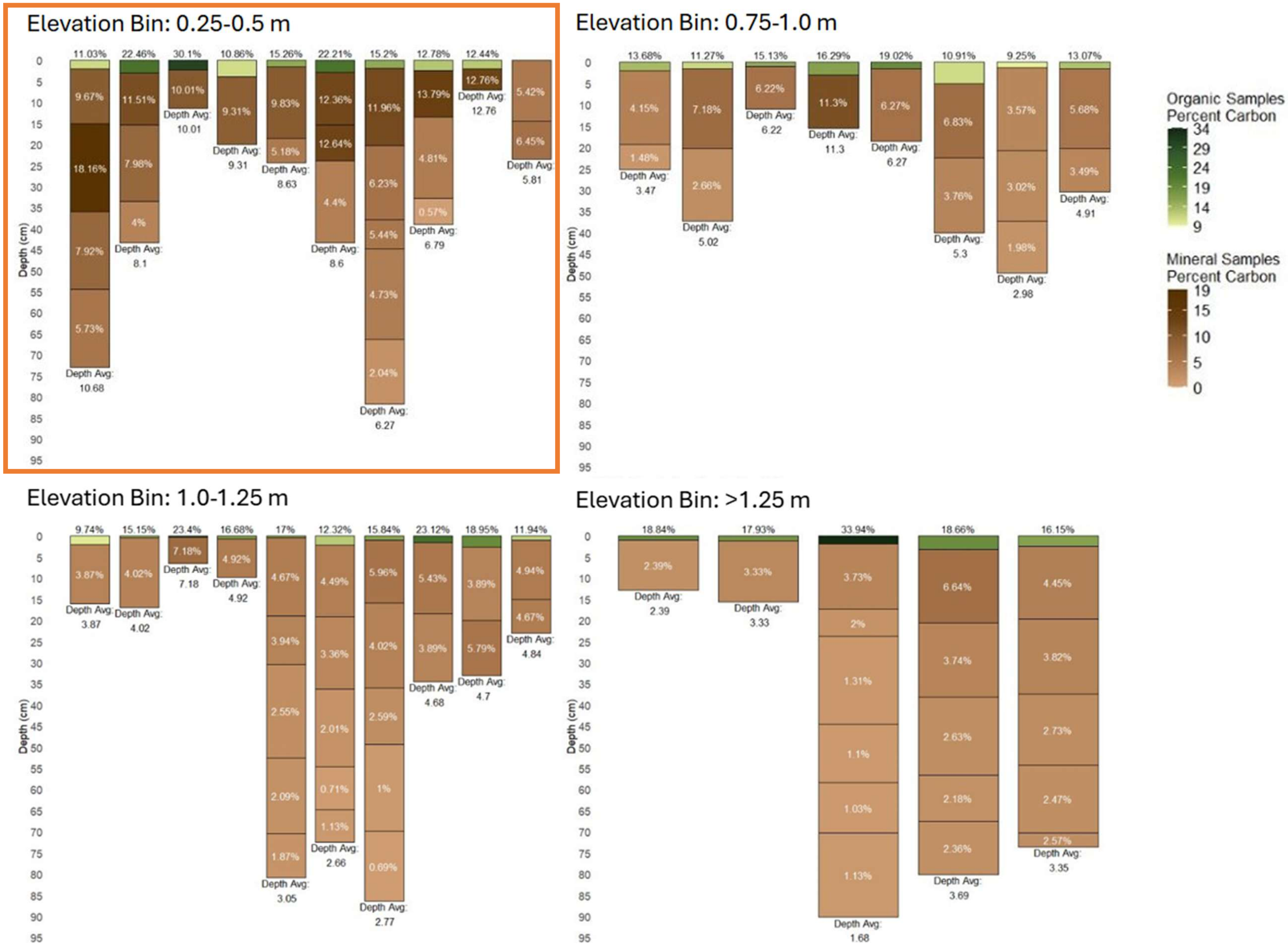

Figure 8. LBC core profiles for elevation bins with significant differences (0.25-0.5 vs. 0.75-1.0 m; 0.25-0.5 vs. 1.0-1.25 m; 0.25-0.5 vs. >1.25 m)

3.2 Hydrodynamic Model Results

3.2.1 Model Calibration and Validation

The calibration and validation of the models resulted in varying RMSE values for the three floodplains (Table 8Table 8). Channel Manning's *n* values for LRV and LE were modified due to the model underperforming in these small and complex headwater streams.

The LRV reach contained two active beaver dams, and similar to the channel Manning's *n* calibration, I iteratively updated the beaver dam area's roughness value until the smallest RMSE was achieved. This occurred at a Manning's *n* of 2.5, a value on the higher side of the range of Manning's *n* values that have been used to represent log jams(Addy & Wilkinson, 2019; Hahn et al., In Review). Beaver's (*Castor canadensis*) pack the upstream side of their dams with mud, decreasing the porosity of the structure, which in turn reduces the amount of flow able to pass through the foundational mass of woody material, causing a backwater affect (Baker & Hill, 2003; Larsen et al., 2021). Therefore, I believe the use of a higher Manning's *n*, which increased modeled WSELs behind the dam, to represent the beaver dam area paired with the SRH-2D obstruction feature was justified.

Removing the calibration points within the beaver dam backwater area resulted in an RMSE of 8 cm for the calibration simulation and 11 cm for the validation simulation, a 4.6 and 4.7 cm difference, respectively. This shows that, outside of the beaver pond areas, the model predicted WSELs more accurately.

For LE, I found that a single roughness value for the entire channel was not appropriate. I first attempted to increase roughness in areas where roughness elements were observed in the field. However, the RMSE values remained large. I observed that modeled WSELs were consistently higher than the in-field measurements for the upstream portion of the channel and lower for the downstream portion. Therefore, to improve the performance of the model two channel *n* values, a smaller upstream and a larger downstream value were calibrated for the LE channel.

Generally, the models performed consistently under the two observed flow rates. The error increased by ~ 3.1 cm for LRV while there was only a ±0.1 cm difference for LBC and LE for the validation simulation. I held the floodplain *n* value constant for both floodplains during the calibration and validation process as overbanking was not observed in the field during WSE data collection and therefore could not be calibrated.

Table 8. Model calibration and validation data for the LBC, LRV, and LE hydrodynamic models

Calibration

Floodplain	Collection Date	Q (cms)	Manning's *n*	RMSE (m)
LBC (Christensen & Morrison, 2026)	--	1.6	Channel: 0.04 Floodplain: 0.0795*	0.10
LRV	06/05/25	0.457	Channel: 0.095 Beaver Dams: 2.5 Floodplain: 0.219	0.126
LE	05/16/24	0.493	Channel US: 0.06 Channel DS: 0.14 Floodplain: 0.16	0.103

Validation

Floodplain	Collection Date	Q (cms)	RMSE (m)
LBC	--	1.0	0.09
LRV	05/30/25	0.405	0.157
LE	06/03/24	0.418	0.104

*In Christensen & Morrison's model, two floodplain roughness coefficients were used, a low (0.1) and a high (0.3) value (Christensen & Morrison, 2026). Alternatively, I used the Arcement & Schneider floodplain roughness estimation methodology to determine the floodplain roughness used in my model simulations (1989).

3.2.2 Model Simulations

The model results show a positive correlation between inundation extent and discharge, see Figure 9. This relationship is illustrated in Figure 10, Figure 11, and Figure 12 for LBC, LRV, and LE, respectively. The 2-year recurrence interval simulation resulted in a minimum area of inundation of 167, 2,780, and 197 m^2 for LBC, LRV, and LE, respectively. The 500-year recurrence interval simulation resulted in a maximum area of inundation of 10,363, 17,678, and 6,171 m^2 for LBC, LRV, and LE, respectively. The number of cores inundated per floodplain varied between flood simulations and elevation bins (Table 9). The LBC flood flows inundated the fewest core locations, 37.5 %, then LRV with 60.4 %, and LE with 72.9 %.

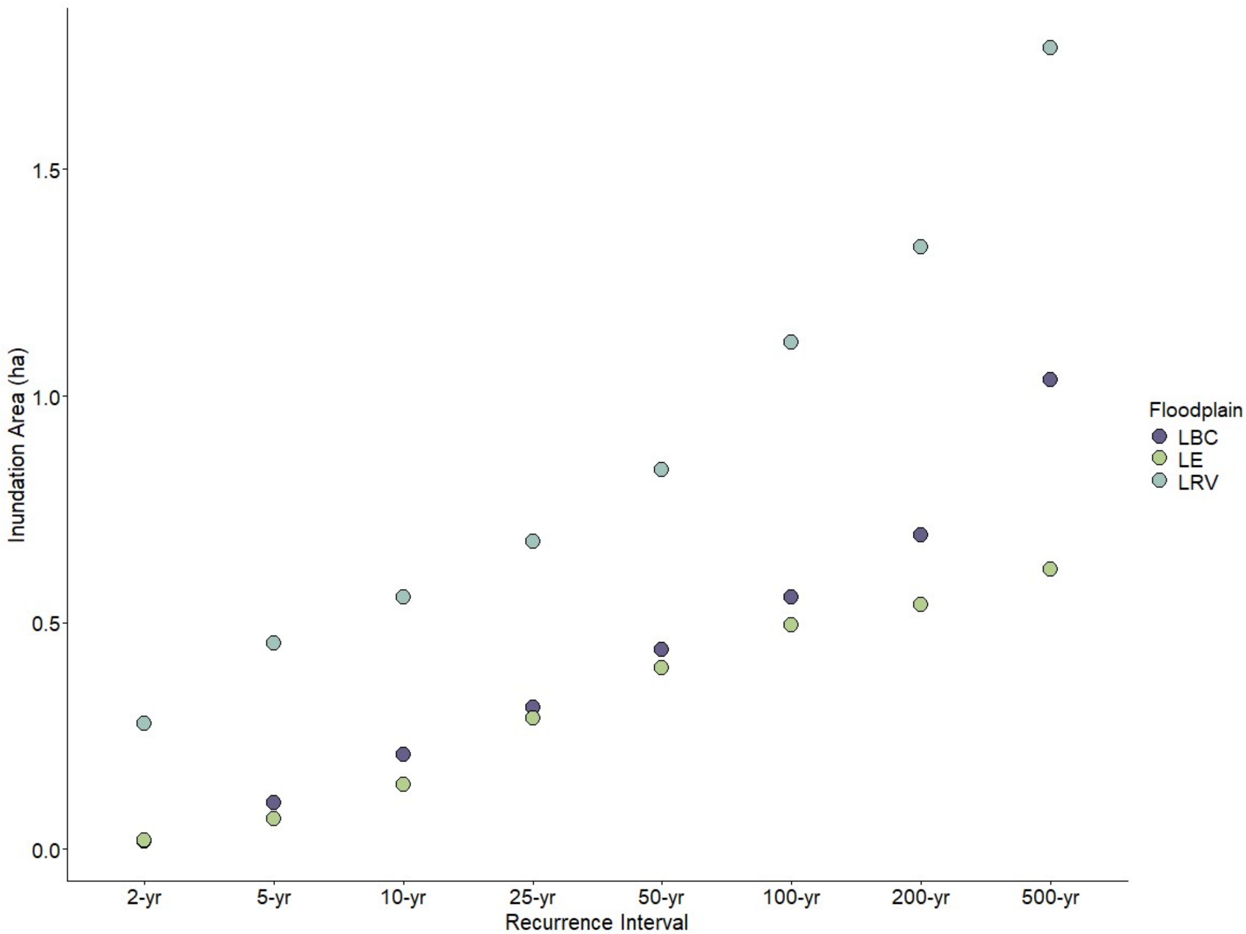

Figure 9. Floodplain inundation area (ha) per floodplain recurrence interval

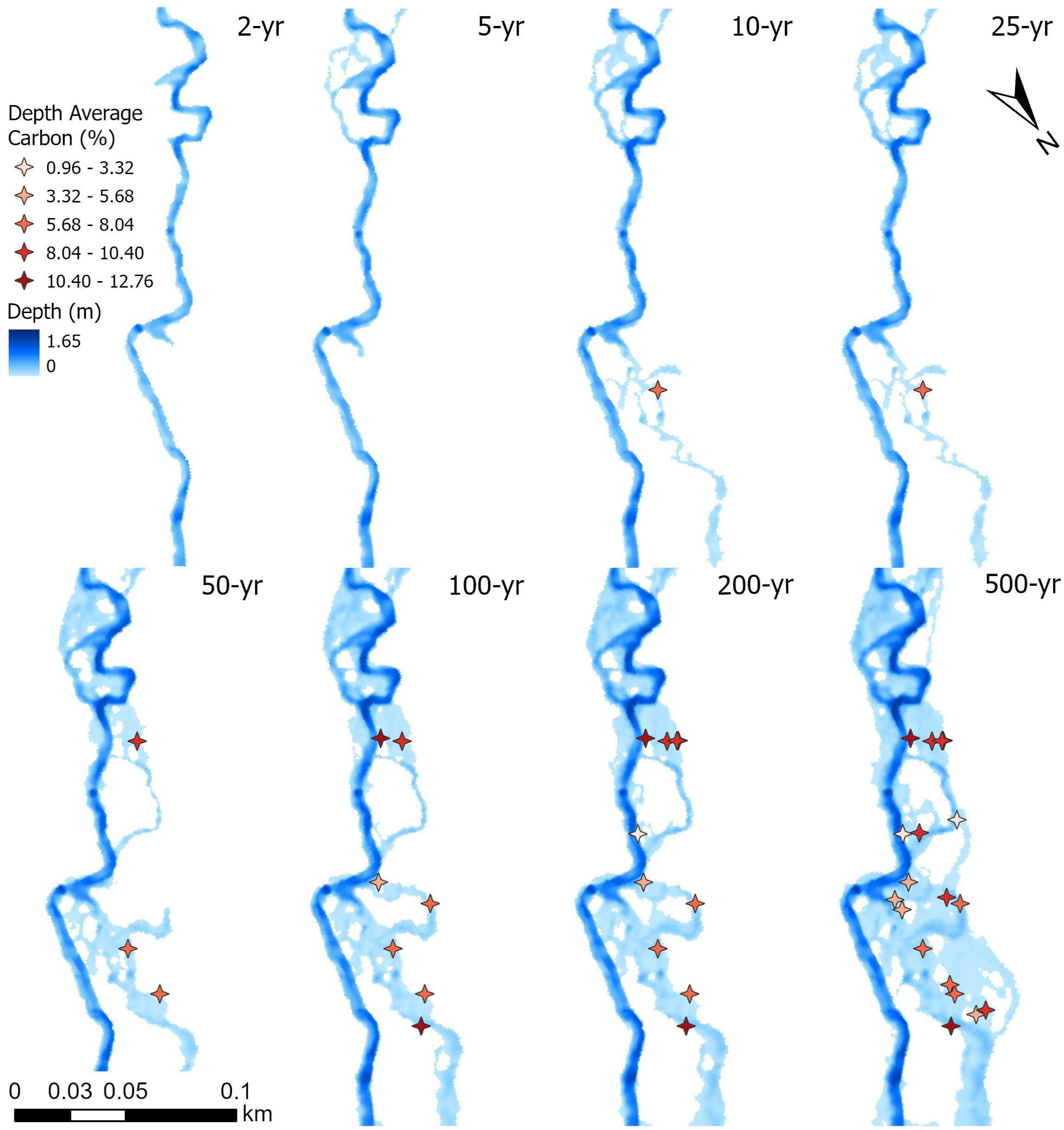

Figure 10. LBC cores inundated at the 2- through 500-yr flood recurrence interval flows and their respective depth-averaged percent SOC

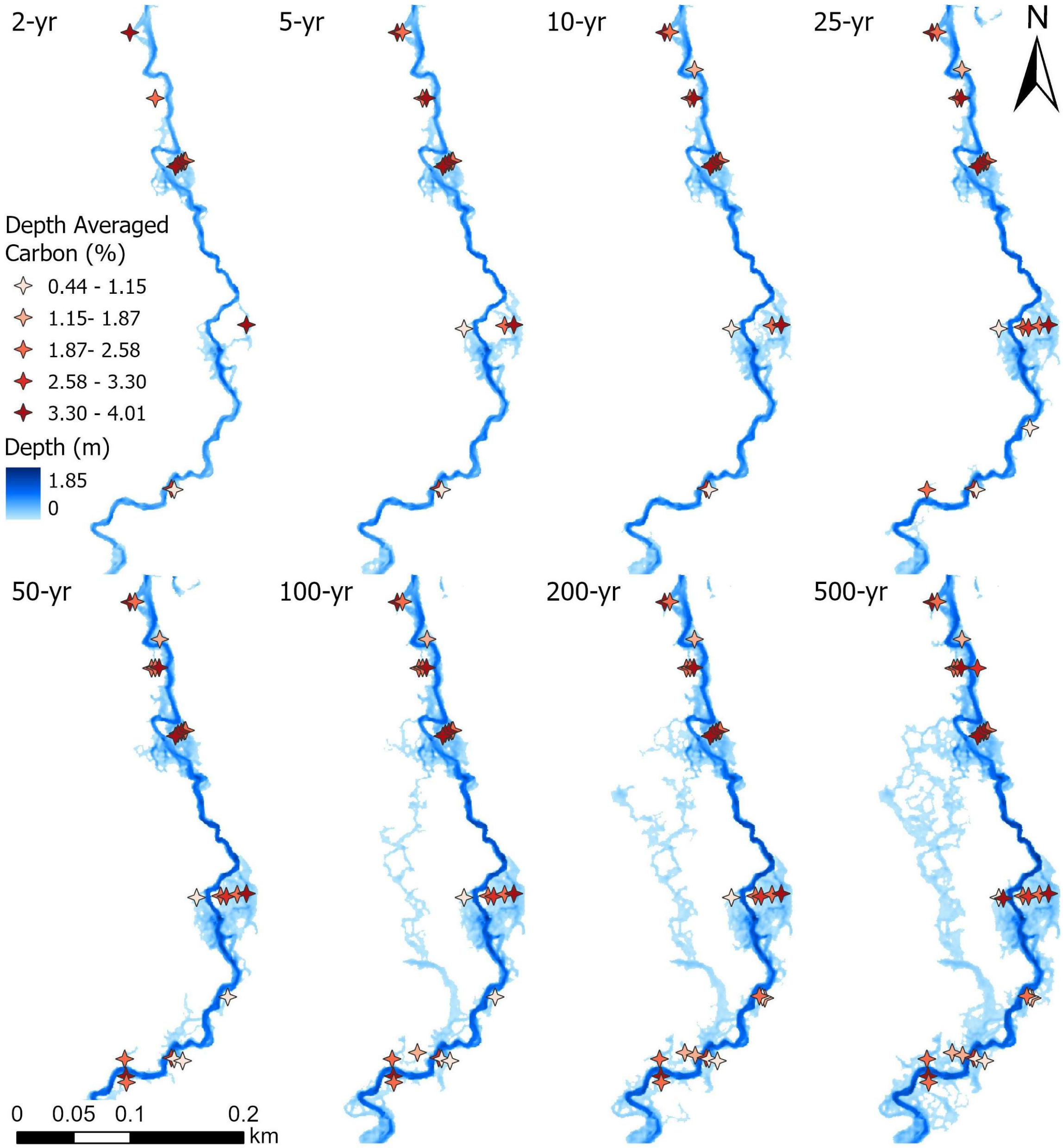

Figure 11. LRV cores inundated at the 2- through 500-yr flood recurrence interval flows and their respective depth-averaged percent SOC

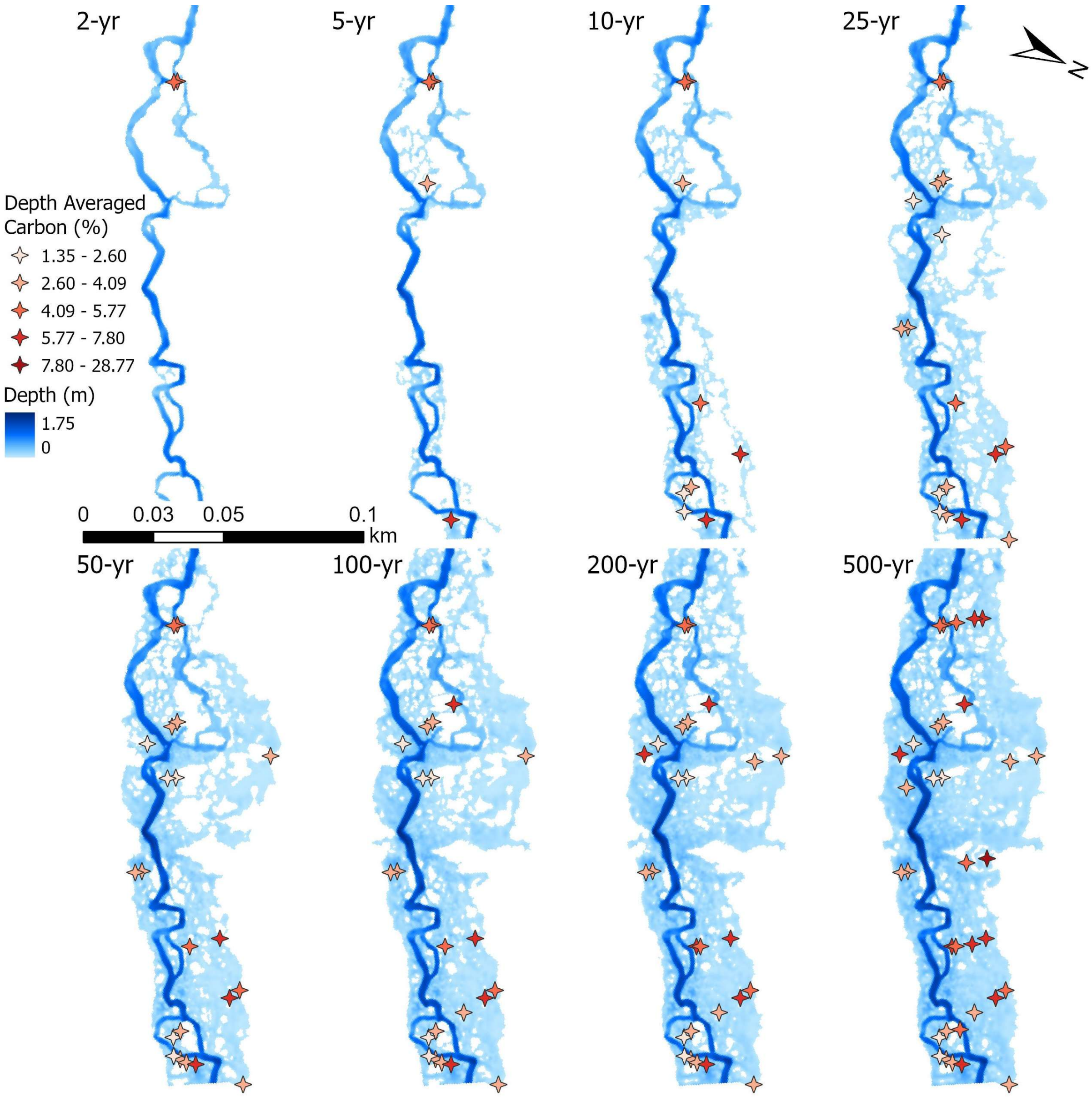

Figure 12. LE cores inundated at the 2- through 500-yr flood recurrence interval flows and their respective depth-averaged percent SOC

Table 9. Number of cores inundated per floodplain, elevation bin, and flood event

	0.00-0.25			**0.25-0.5**			**0.5-0.75**			**0.75-1.0**			**1.0-1.25**			**>1.25**			**Total**		
	LBC	**LRV**	**LE**	**LBC**	**LRV**	**LE**	**LBC**	**LRV**	**LE**	**LBC**	**LRV**	**LE**	**LBC**	**LRV**	**LE**	**LBC**	**LRV**	**LE**	**LBC**	**LRV**	**LE**
No. of cores per elev. bin	8	5	8	10	10	9	7	8	5	8	7	10	10	11	8	5	7	8	48	48	48
2-year	--	3	1	--	4	1	--	2	--	--	1	--	--	--	--	--	--	--	0	10	2
5-year	--	3	2	--	6	1	--	2	1	--	2	--	--	1	--	--	--	--	0	14	4
10-year	--	3	5	--	6	3	1	3	1	--	2	--	--	1	--	--	--	--	1	15	9
25-year	--	3	7	--	6	5	1	4	3	--	3	1	--	2	1	--	1	--	1	19	17
50-year	--	3	7	2	7	7	1	6	3	--	4	2	--	2	1	--	1	1	3	23	21
100-year	1	3	7	4	7	7	2	6	3	--	5	3	--	2	1	--	1	2	7	24	23
200-year	1	3	8	6	7	7	3	6	4	--	6	4	--	4	2	--	1	2	10	27	27
500-year	5	3	8	7	7	9	4	7	4	2	6	9	--	5	2	--	1	3	18	29	35

3.2.3 Relationships Between SOC and Inundation Discharge

Grouping cores by their initial inundation discharge does not show a clear pattern in SOC content. Figure 13 presents the summary statistics for the mineral-only dataset, including both individual sample values and depth-averaged percent carbon for cores grouped by initial inundation discharge for each floodplain. Cores were grouped based on their initial inundation discharge since the cores that are inundated at the 2-yr recurrence interval flood were also inundated at the 5-, 10-, 25-yr, etc. floods, so frequency of inundation would be highest for areas flooded at lower discharges. While a clear pattern does not emerge, larger floods (Individual samples: LBC = 100-yr, LE = 200-yr, LRV = 50-yr; Core averaged: LBC = 200-yr, LRV = 500-yr, LE = 500-yr) appear to have the highest percentage of SOC on average for both datasets. There appears to be a bimodal distribution for both individual samples and entire cores for the LE and LRV floodplains, but the LBC data do not confirm this pattern due to the lack of cores initially inundated by the 2-, 5-, or 25-yr recurrence interval floods.

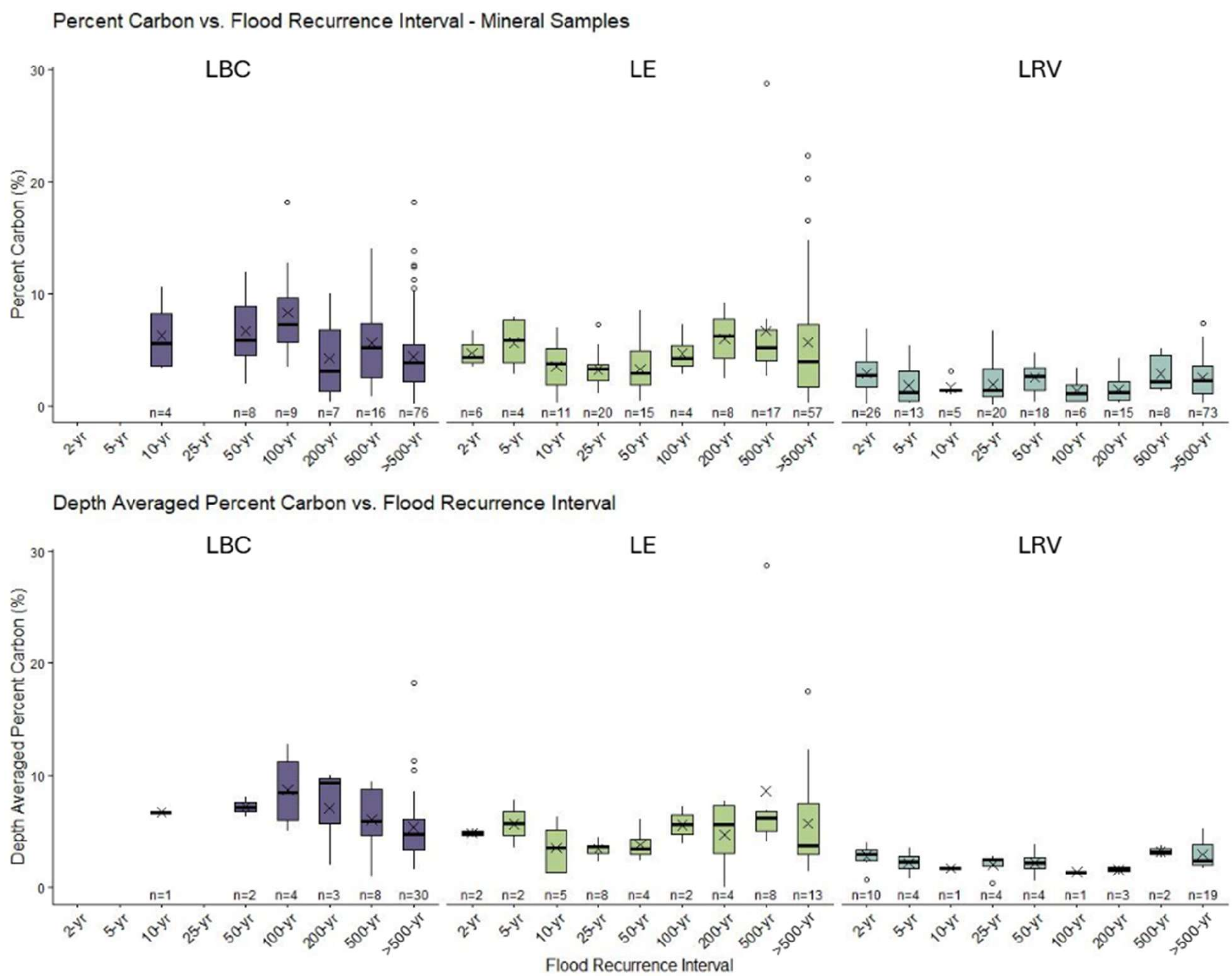

Figure 13. Top panel summary statistics for mineral-only individual samples grouped by initial inundation discharge at LBC, LE, and LRV (from left to right). Bottom panel, summary statistics for depth-averaged percent carbon grouped by initial inundation discharge at LBC, LE, and LRV (from left to right). The horizontal lines within the boxes represent the medians, the x marks the mean, and the hollow dots show outlier samples.

To determine whether percent carbon differed between cores grouped by initial inundation discharge, I performed the non-parametric Kruskal-Wallis test and the pairwise Wilcoxon rank-sum test. The conditions required to perform the Shapiro-Wilk test (n = 3) were not met due to small sample sizes within groups, and therefore normality was not assessed at this level. I identified statistically significant differences in percent carbon ($p \leq 0.05$) for the LE full individual sample dataset ($\chi^2 = 16.35$, df = 8, p = 3.77e-02) and for the mineral-only dataset at

LBC ($\chi^2 = 13.20$, df = 5, p = 2.16e-02), LRV ($\chi^2 = 17.27$, df = 8, p = 2.74e-02), and LE ($\chi^2 = 15.54$, df = 8, p = 4.94e-02). However, the results of the pairwise Wilcoxon rank-sum test did not support these findings. While the Kruskal-Wallis test suggested there were statistically significant differences for the mineral-only LBC and LRV datasets, none of the adjusted p-values met that criteria ($p \leq 0.05$). At LE, only one comparison, between the 25-yr and 500-yr recurrence intervals, showed significant differences for both the full and mineral-only datasets. I performed the Kruskal-Wallis test on core depth-averaged percent carbon grouped by initial inundation discharge. With this restricted dataset, recurrence interval bins commonly contained $n \leq 3$ and all but one result lacked statistical significance. Based on the limited and inconsistent differences in the pairwise comparisons, inundation frequency appears to be a weak predictor of SOC content across these floodplains.

3.2.4 Relationships between Carbon Stocks and Inundation

Carbon stock was calculated at each floodplain for all recurrence interval inundation extents. This was done cumulatively instead of per initial inundation discharge as was previously analyzed to include all carbon measurements within the inundated area.

Carbon stock is frequently reported in terms of a depth of 1 m (Hinshaw & Wohl, 2023; Ladd et al., 2022; Lininger et al., 2018). Extrapolating all cores to a depth of 1 m may overestimate SOC content due to the documented relationship of decreasing SOC storage with increasing soil depth (D'Elia et al., 2017; Jobbágy & Jackson, 2000). However, due to the hydrologic variability and association of nutrient-rich sediment aggradation and burial of OM layers (Gurwick et al., 2008), the strength of this relationship is weaker in floodplains than other ecosystems, as substantiated in core depth profiles at all study sites.

Carbon stock calculations do not include the organic layer samples, due to the isolation of the fine soil fraction (i.e., using the hybrid BD for stock calculations, Eq. (2)), to reduce the chance of SOC overestimation (Reed et al., 2022; Throop et al., 2012). Table 10 shows the carbon stock statistics for the entire data set and each floodplain's dataset. These have been broken up into the active layer stocks and the stock extrapolated down to 1 m. For the 1 m extrapolated stock statistics, the actual depth sampled was used for cores that were halted due to the presence of bedrock and/or coarse alluvium while cores that were halted due to high soil saturation were extrapolated out to 1 m, the same methodology employed by Lininger et al. (2019). The extrapolation increased the amount of SOC stock at each floodplain, but it did not affect the relative order of carbon content between floodplains. LBC had the lowest carbon stock, while LE had the highest for both the active layer and extrapolation. The stock results conflicted with the percent carbon results in that LBC was shown to have the highest percent carbon of the three floodplains studied while the opposite is true for the stock data. The incongruous results highlight the importance of considering floodplain-specific soil properties when evaluating SOC storage.

Table 10. Carbon stock using hybrid BD* statistics for the active layer versus extrapolated to 1 m in depth

Dataset	Number of cores extrapolated	Min (Mg C/ha)	Max (Mg C/ha)	Mean ± SE (Mg C/ha)	Median (Mg C/ha)
Complete - Active	NA	0.00	506.07	128.35 ± 6.59	119.82
Complete – 1 m	36	0.00	585.06	169.82 ± 9.98	146.23
LBC - Active	NA	7.66	304.16	107.25 ± 9.79	109.19
LBC – 1 m	2	7.66	421.20	113.16 ± 11.73	109.19
LRV - Active	NA	11.57	275.08	123.10 ± 8.38	116.73
LRV – 1 m	17	11.57	342.72	159.61 ± 12.64	155.07
LE - Active	NA	0.00	506.07	154.69 ± 14.33	141.08
LE – 1 m	17	0.00	585.06	236.69 ± 21.11	217.17

*Carbon stock statistics using the total BD, Eq. (1), are included in Appendix E: Total Bulk Density Active Layer Organic Carbon Stock Statistics for comparison purposes.

The SOC stock extrapolated to 1 m was used to calculate the cumulative carbon stock based on all cores inundated at each recurrence interval discharge. Figure 14 shows the mean carbon stock trends across recurrence intervals and the associated number of cores inundated. The mean carbon stock at LBC and LE show considerable variability, whereas LRV exhibits a more consistent trend with the number of cores inundated increasing consistently. Peak carbon stock occurs at the cores inundated by the 50-, 25-, and 2-yr recurrence interval discharges for LBC, LRV, and LE, respectively.

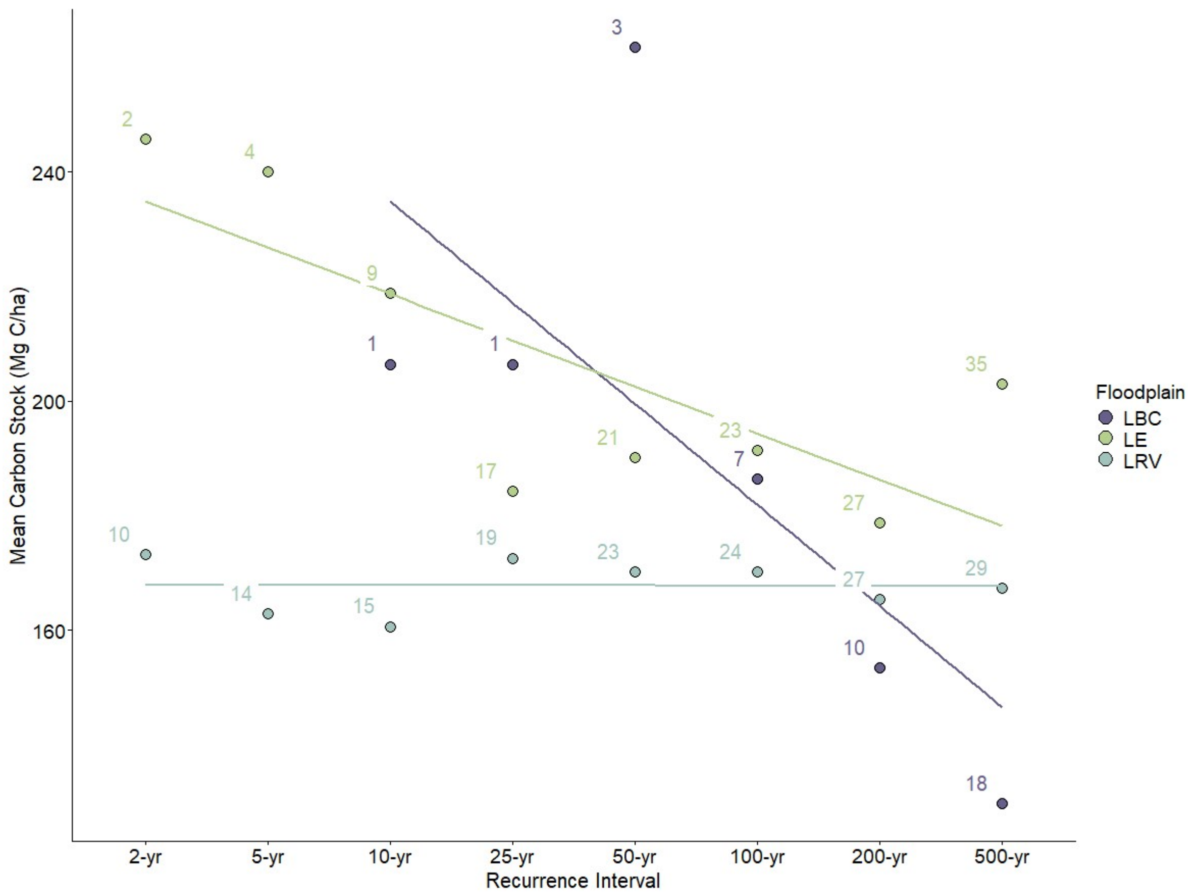

Figure 14. Carbon stock trends across recurrence intervals for LBC, LRV, and LE. The number of cores inundated at each recurrence interval is shown for each floodplain in the corresponding color.

To compare the carbon stock for each recurrence interval between floodplains, I needed to normalize the data by the modeled reach length. Therefore, instead of presenting average mass of carbon per recurrence interval inundation, which would result from multiplying the inundated area by the mean carbon stock, the carbon mass per unit length was calculated for each recurrence interval using Eq. (10). Figure 15 provides the trends in carbon mass per unit length for each floodplain's recurrence interval flows. For all floodplains there is a positive relationship between mean carbon mass per unit length and recurrence interval inundation. This result makes sense due to the positive relationship between area of inundation and discharge.

$$\frac{C\ mass}{reach\ length}\left(\frac{Mg\ C}{m}\right) = \frac{Mean\ C\ stock\ \left(\frac{Mg\ C}{ha}\right) * Recurrence\ Interval\ Inundation\ Area\ (ha)^{**}}{reach\ length\ (m)} \tag{10}$$

**Recurrence interval inundation area was calculated by subtracting the calibration flow area from the flow area associated with each recurrence interval. Flow area in both cases was determined as the number of cells with modeled flow multiplied by the pixel area.

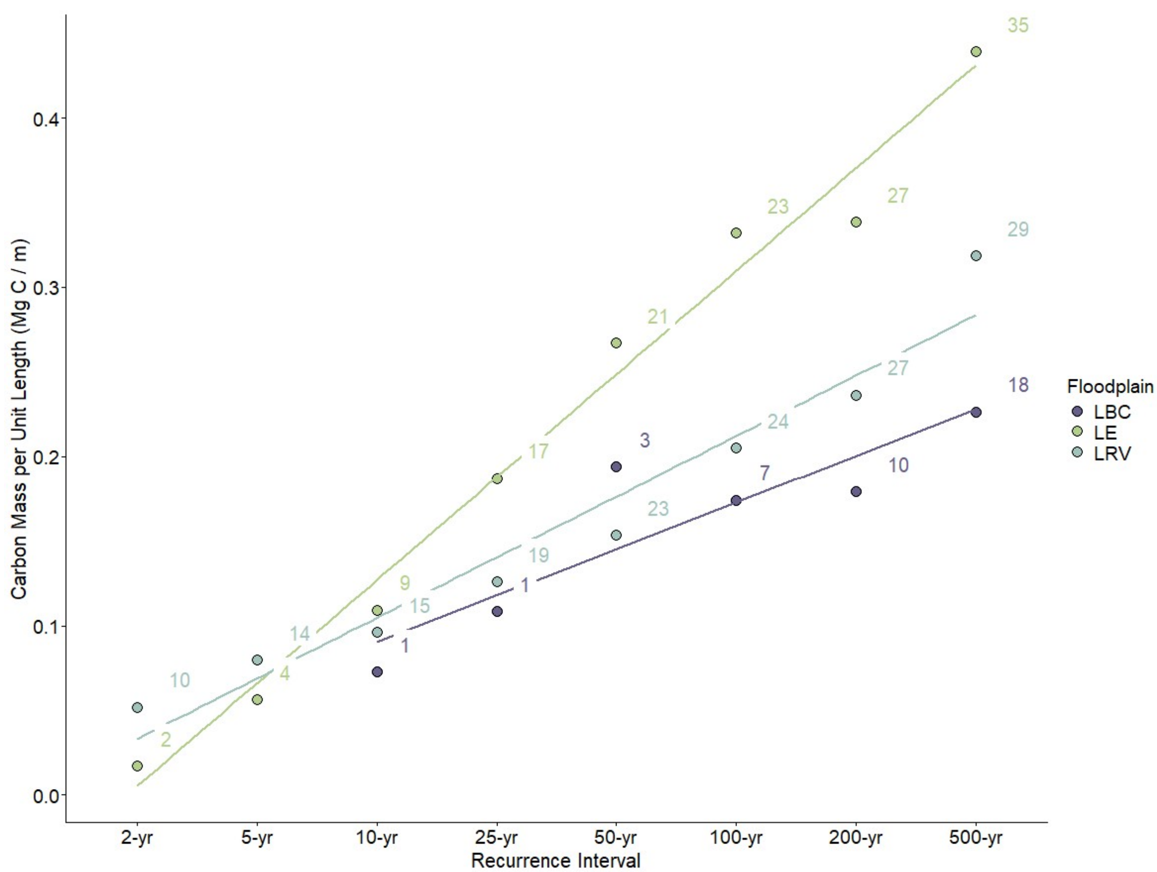

Figure 15. Carbon mass per unit reach length trends across recurrence intervals for LBC, LRV, and LE. The number of cores inundated at each recurrence interval is shown for each floodplain in the corresponding color.

4. DISCUSSION

Channel restoration intended to reconnect the channel with the floodplain has been proposed as a novel carbon reduction strategy. However, with limited information on the timescale or magnitude of SOC storage in these floodplain systems, this proposal may be invalid. The three floodplains studied are slated for LTPBR, which will include the installation of BDAs and PALs. In a recent study, a beaver-dam-influenced wetland in Switzerland was found to store a larger magnitude of carbon than those unmodified (Hallberg et al., 2026). Therefore, the hydraulic effects of BDAs (which are meant to mimic beaver dams) in increasing lateral connectivity and groundwater table elevation (Bouwes et al., 2016; Jones et al., 2026) could result in increased floodplain carbon storage. However, Scamardo & Wohl (2020) found that there was not a statistically significant groundwater response within one year of the installation of BDAs on two Colorado headwater streams. Understanding that the hydraulic impact of these structures, which is their primary objective, may vary makes it clear that their effect on SOC storage may also vary and that there are likely other floodplain-specific factors that will have a larger influence. Although this study only considers pre-restoration conditions, quantifying SOC stored in areas flooded at varying frequencies helps assess the relationship between inundation frequency and floodplain SOC storage, as floodplains will likely experience increased inundation with the installation of LTPBR structures.

4.1 Floodplain SOC Content

The mineral SOC contents measured at LBC, LRV, and LE were smaller than average mineral SOC measured at climatically similar wetlands in Colorado (Daugherty et al., 2019). Comparing the three floodplains studied shows that LBC has the highest amount of SOC stored when considering the depth-averaged percent carbon. This dataset only considers the active layer percent carbon, without consideration for bulk density or extrapolation. When looking at the depth-averaged percent carbon data compared to relative surface elevation above the channel, the low R^2 (LBC = 0.26, LRV = 0.08, LE = 0.02) values indicate that relative surface elevation above the channel may be a weak predictor of SOC content. Sutfin & Wohl (2017) found there was not a significant relationship between percent carbon and relative surface elevation to the channel in similar systems. Based on the p-values (LBC = 1.94e-4, LRV = 0.051, and LE = 0.383), the negative linear relationship between depth-averaged percent carbon and relative surface elevation to the channel observed for LBC and LRV is stronger than the positive linear relationship seen at LE. The p-value ($p \leq 0.05$) for the LBC depth-averaged cores suggests that there is a negative linear relationship between relative surface elevation and depth-averaged carbon. However, the lack of validation from LE and LRV makes it difficult to accept or reject the null hypothesis.

Considering the statistics calculated on the depth-averaged percent carbon dataset, only LBC and LRV had statistically significant differences ($p \leq 0.05$) between elevation bins. LBC had three elevation bin comparisons that yielded significant differences (0.25-0.5 m vs. 0.5-0.75 m, 0.25-0.5 m vs.1.0-1.25 m, and 0.25-0.5 m vs. >1.25 m) while LRV only had one (0.25-0.5 m vs. 1.0-1.25 m). All elevation bin comparisons that had significant differences occurred between cores in the 0.25-0.5 m elevation bin and a higher elevation bin.

The LBC soil core profiles (Figure 8) show that the 0.25-0.5 m elevation bin has much higher amounts of carbon, specifically the top 20-30 cm of the mineral cores. In comparison, the 0.75-1.0 m, 1.0-1.25 m, and >1.25 m elevation bin cores exhibit much lower percent carbon values at the same depth. The lower relative elevation bins at LBC (0.0-0.25 m and 0.25-0.5 m) were characterized with dense vegetation cover, while moving away from the channel and onto the relict floodplain (relative elevation increased) corresponded with a shift in vegetation to short, dry grasses. The vegetation transition between the lower and higher relative elevations at LBC and LE was apparent. It has been shown that vegetation type influences SOC storage through litterfall rates and root growth, which are heavily influenced by annually and seasonally variable soil moisture and temperature (Jobbágy & Jackson, 2000; Kögel-Knabner, 2002; Rieger et al., 2015). The lack of difference between elevation bins at LE is likely due to topographic variability across the floodplain, leading to fewer samples collected on the drier terrace (i.e., areas of higher elevation were located within the densely vegetated floodplain). Therefore, the vegetation disparity may be a primary factor influencing the statistically significant differences between elevation bins at LBC.

The statistical difference between the 0.25-0.5 m vs. 1.0-1.25 m elevation bins at LRV may be due to depth of sampling rather than actual differences in SOC content. The ranges in percent carbon values for the topmost mineral core in both elevation bins are comparable (0.25-0.5 m: 2.54-6.19%; 1.0-1.25 m: 1.6-5.36%). The major difference between the two elevation bins is the terminal coring depth. Only one core out of ten in the 0.25-0.5 m elevation bin reached a depth of 70 cm or greater, while seven out of eleven cores in the 1.0-1.25 m elevation bin reached this depth or greater. As discussed previously, SOC content decreases with depth, therefore the statistical difference may not be a result of relative surface elevation above the channel, but instead a factor of terminal core depth (Heger et al., 2021; D'Elia et al., 2017; Jobbágy & Jackson, 2000).

4.2 Model Simulations

The hydrodynamic model results provide an approximation of the expected inundation area for each of the floodplains at the 2- through 500-yr recurrence interval floods. The areas of inundation were used to determine if there was a relationship between SOC content and inundation frequency. Looking at Figure 9, we can see that as flood flows increase, the area of inundation increases. Figure 10, Figure 11, and Figure 12 depict that flood flows follow the same path but extend past the previous inundation area with increasing discharge. Therefore, cores that were inundated by the 2-yr flows were also inundated at the 5-, 10-, 25-, etc. yr recurrence interval discharge.

The flow paths for all three floodplains initially stayed within floodplain-spanning secondary channels, but as flows increased, overland flow began to occur. Looking at Figure 10, Figure 11, and Figure 12 we can see that floodplain overland flow varies between LBC, LRV, and LE. The LRV channel appears to be more disconnected from the floodplain than LE or LBC due to the flow remaining almost entirely within the channel and secondary channels up to the 500-yr flow rate, except for the areas around the beaver dams. The channel banks experienced significant incision along the middle portion of the modeled reach, supporting the lack of inundation (Figure 11). In comparison, the LE channel appears to be the most connected with the floodplain. Extensive overland flow occurs at the 25-yr flow rate. The initiation of overland flow at a much lower flow rate may be a result of the LE secondary channel activation at low flows. The secondary channels were actively flowing at calibration ($Q = 0.493$ cms) and validation ($Q = 0.418$ cms) discharges. The holding capacity of LRV's secondary channels is likely greater than at LE due to the lack of water in these depressed areas at low flows. Therefore, the limited capacity within the LE secondary channels may contribute to the initiation of overland flow at a much lower recurrence interval discharge.

An important aspect of the LRV model to consider is the beaver dams. The floodplain areas surrounding the beaver dams show inundation increasing with discharge. The occurrence of the larger recurrence interval discharges may damage or destroy the beaver dams and therefore reduce their backwater effects (Wohl et al., 2019). This may result in the cores inundated at the lower recurrence interval discharges due to the beaver dam's presence, not being inundated at larger flows. However, the conditions of failure are not well understood (Brazier et al., 2021). While the methodology used to simulate the beaver dams was based on previous studies (Schultz et al., 2025), additional research/model development is necessary to accurately represent these natural features under a range of flow rates.

Table 9 provides the distribution of cores inundated per elevation bin and recurrence interval flood. A larger portion of cores were generally inundated in the lower elevation bins for all recurrence interval discharges. In the lowest elevation bin (0.0-0.25 m) 5/8, 3/5, and 8/8 of the cores were inundated at the 500-yr recurrence interval discharge for LBC, LRV, and LE, respectively. At the highest (>1.25 m) 0/6, 1/7, and 3/8 cores were inundated at the 500-yr recurrence interval discharge for LBC, LRV, and LE, respectively. The higher proportion of cores inundated in lower elevation bins reflects the expected hydrologic pattern in which floodwaters initially occupy lower-lying topography and expand laterally and vertically into higher elevations as discharge and flow depth increase until the flood peak. However, at LBC and LRV a larger proportion of the cores in the 0.25-0.5 m elevation bin were inundated at the 500-yr recurrence interval discharge compared to the 0.0-0.25 m. Similarly, the 0.75-1.0 m elevation bin had a larger proportion of cores inundated than the 0.5-0.75 m elevation bin at LE.

This suggests that relative elevation does not solely predict inundation. The spatial variability in floodplain topography can produce low-lying areas distant from the channel that may not experience inundation at a given discharge.

The spatial distribution (Figure 10, Figure 11, and Figure 12) of inundated cores over the range of simulated discharges does not reveal a relationship between depth-averaged SOC content and inundation frequency. However, there appear to be areas of high carbon content spaced heterogeneously. As described in the introduction, floodplain microtopography creates differing effects from flood flows due to surface and vegetation variability. The hot spots of cores with higher depth-averaged percent carbon are likely due to a combination of localized factors rather than frequency of inundation (Daugherty et al., 2019).

4.2.1 Relationships Between SOC and Inundation Discharge

When comparing the percent carbon across cores grouped by their initial inundation discharge recurrence interval, peak SOC storage differed between the floodplains (Figure 13). Median values suggest that peak percent SOC content occurs in soils flooded at intermediate to high recurrence intervals (100-yr at LBC, 50-yr at LRV, and 200-yr at LE) (Figure 13 - top panel). When considering each core using a depth-averaged percent carbon, peak SOC content occurs in soils flooded at high recurrence interval flows (200-yr at LBC, 500-yr at LRV, and 500-yr at LE) (Figure 13 - bottom panel). However, these peaks are not consistent when considering all summary statistics.

When considering the results presented in Figure 13, it is important to remember that only the cores that were initially inundated under the respective recurrence interval flows were considered for each grouping. The summary statistics either use individual mineral samples or each core's depth-averaged percent carbon, but for this discussion, I will focus on the depth-averaged percent carbon summary statistics (Figure 13 - bottom panel).

LBC's 200-yr recurrence interval SOC peak is driven by two of the three cores skewing the data towards the higher range of depth-averaged percent carbon values measured. However, the mean peak occurs at the 100-yr recurrence interval flow because at this inundation two of the cores exhibit some of the highest depth-averaged percent carbon values. The difference in peaks is due to the small sample sizes. Two other cores with high carbon content are never inundated, suggesting that localized soil conditions rather than inundation may play a larger role in SOC storage, as illustrated in Figure 10, Figure 11, and Figure 12.

The cores inundated at LRV's and LE's 500-yr recurrence interval result in the peak median and mean percent SOC. Similar to LBC, the cores at LRV containing the highest depth-averaged percent carbon (n = 4) occur in areas never inundated, which bolsters the idea that infrequent or lack of inundation may coincide with environmental conditions favorable to SOC storage. The occurrence of peak SOC content in the cores initially inundated by the 500-yr recurrence interval discharge and cores "never" inundated may be due to floodplain plant OM remaining on the floodplain and its incorporation into the soil rather than being transported elsewhere by flood waters (Gervais-Beaulac, 2013; Saint-Laurent et al., 2014, 2016). The SOC content peaking in the areas of infrequent inundation go against the findings presented by Sutfin, Bai, and Yin, which show a positive correlation between SOC content and soil moisture (Bai et al., 2020; Sutfin & Wohl, 2017; Yin et al., 2019). While frequency of inundation does not directly reflect soil moisture, areas of frequent inundation would be wetted during these events, resulting in increased soil moisture.

However, the summary statistics at LRV and LE exhibit a bimodal distribution. The second peak occurs for cores initially inundated at the 2-yr and 5-yr recurrence interval discharge for LRV and LE, respectively. A potential reason may be due to the soil moisture in these areas hindering the release of CO_2 through microbial decomposition of plant matter or increasing plant primary productivity. The increased input of OM from enhanced primary productivity may outweigh the redistribution of surficial litter from frequent inundation. The bimodal distribution is not apparent at LBC because of an absence in cores initially inundated at the smaller recurrence interval discharges.

Depth-averaged percent carbon paired with recurrence interval of initial inundation discharge does not provide a clear pattern, nor does the number of samples composing each group provide statistical strength. However, from the limited data, soils inundated at either high, 2- through 5-yr, or low frequencies, 200- through 500-yr, appear to contain the highest percentage of carbon.

4.2.2 Relationships between Carbon Stocks and Inundation

Carbon stock provides important context when comparing SOC content between floodplains. The calculation includes each sample's bulk density (BD), accounting for each floodplain's compaction and resulting in a variable mass of soil per unit volume multiplied by each sample's percent carbon. In addition to BD, the cores in Figure 14 and Figure 15 were extrapolated down to 1 m in depth when coring was terminated due to saturation (LBC n = 2, LRV n = 17, LE n = 17). The range of mean SOC stocks calculated in this study (113.16 – 236.69 Mg C/ha) fall within the range of values found in similar systems (Wohl & Knox, 2022).

There are inherent sources of uncertainty present within the stock calculations. One of those sources is the methodology of calculating BD from individual cores rather than the

USDA’s methodology (USDA Soil Quality Institute, 2001). I calculated individual sample hybrid BD, which has been found to overestimate BD if compaction during the coring process occurs (Lang et al., 2025). To minimize core compaction, I measured depth between each core collected and attempted to core in 18 cm increments. While this error may be present within the data, the individual sample BD includes the variability of soil compaction longitudinally/laterally and with depth across the floodplain, better representing this alluvially influenced land area within the stock data (Iqbal et al., 2005).

The extrapolation to 1 m likely overestimated carbon content because SOC content decreases with depth (D’Elia et al., 2017; Jobbágy & Jackson, 2000), but the strength of this trend decreases due to the alluvial processes that influence floodplains (Gurwick et al., 2008). While carbon may be overestimated, not including the extrapolation would greatly underestimate the SOC content at LRV and LE as deeper soils unable to be collected still contain SOC. Thirty-five percent of the cores sampled at LRV and LE could not be cored to 1 m due to saturation. Cores halted due to coarse alluvium (coarse sand, gravels, and cobbles) or bedrock were not extrapolated because I assumed that the SOC content below this depth was negligible (Lininger et al., 2019; Lininger & Polvi, 2020). Lininger et al. (2019) also found that the exclusion of the > 2 mm soil fraction in SOC stock calculations underestimates these values by 15-20%. Therefore, considering floodplain SOC content’s variability with depth overestimates SOC and the exclusion of the > 2 mm soil fraction underestimates SOC, the inclusion of extrapolated data for cores terminated due to saturation was deemed reasonable for stock calculations.

Climate and geology are major controls on a system’s SOC storage capacity. These major controls can be refined into more specific factors (i.e., soil moisture, soil texture, plant communities, aggregate formation, etc). I will be focusing on soil moisture and soil texture in this discussion, as all three floodplains sit at similar elevations (2,435 - 2,675 m) within Colorado's northern Rocky Mountains, resulting in comparable climates. Considering these factors helps us to understand why SOC content varies between LBC, LRV, and LE.

4.2.2.1 Soil Moisture

An important factor in SOC storage is the moisture content of the soil. Soil moisture can both help and/or hinder the microbial decomposition of SOC, leading to the mineralization of organic carbon into CO_2. All three floodplains experience similar flow hydrographs. The Colorado Rockies receive the majority of their precipitation as snow in the winter months (Doesken et al., 2025). The snow accumulates through the cold winters, reducing stream flows. In the late spring/early summer, snowmelt peaks and partitions into overland flow to surface waters and subsurface percolation that recharges groundwater. Similar to the snowmelt-dominated hydrograph profiles, groundwater tables peak in the late spring/early summer. The groundwater table declines throughout the dry season, supporting headwater stream baseflows, with late summer convective thunderstorms supplementing groundwater recharge and streamflow (Westbrook et al., 2011).

Field work occurred during the 2024 and 2025 summer season, with LBC core collection occurring in July-September 2024, LRV core collection in July 2025, and LE core collection in June and July 2025. LE was the earliest to be sampled of both field seasons. The first core collection attempt resulted in many incomplete cores due to soil saturation (n = 12/29, 41.4%). I returned to LE later in the summer and experienced fewer saturated coring locations (n = 5/25, 20%). The field experience at LE illustrates the potential seasonal variability in groundwater table elevation/soil moisture conditions that occur at floodplains.

The soil saturation observed at LE may be an important factor in its comparatively large SOC stocks. The soil moisture conditions likely contributed to the prolific plant growth observed in the field (Rieger et al., 2015). Riparian plants contribute significantly to SOC content through inputs of aboveground litter and belowground roots which decompose and are incorporated into the soil (Blazejewski et al., 2005; Tufekcioglu et al., 2003). Compounding that, the high groundwater table/soil saturation may provide conditions that hinder microbial decomposition of SOC, allowing the soil to retain the carbon input by the non-water limited plant population (Ise et al., 2008; Yin et al., 2019).

4.2.2.2 Soil Texture and Bulk Density

Floodplains are heavily influenced by alluvial processes. Flood flows can aggrade or degrade the floodplain by depositing nutrient-rich sediments or scouring the top sediment layer and surficial plant matter. Flows are reduced when they overbank and move across the rougher, relative to the channel, floodplain surface (Diehl et al., 2023; Sutfin et al., 2021). Slower velocities allow for sedimentation or scour to occur heterogeneously across the floodplain (Wolman & Leopold, 1957). Due to these processes, sediment profiles and textures within a floodplain will have large variation spatially and temporally.

The positive relationship between SOC storage and prevalence of small soil particles, silts and clays, has been thoroughly documented (Cheng et al., 2024; Graf-Rosenfellner et al., 2016; Hassink & Whitmore, 1997; Sutfin & Wohl, 2017; Yin et al., 2019). The soil texture results show that the LE floodplain has the largest percentage of fines while LRV has the smallest (Table 4). SOC content is not solely dependent on the concentration of fines; otherwise, LRV would have the smallest SOC stock. Combining the texture data with each floodplain's BD may provide more insight into the relative hierarchy in SOC stocks for the studied floodplains.

BD represents the mass of dry soil within a specified volume. A larger BD corresponds with greater compaction and reduced pore space, which could correspond with a smaller fraction of OM (SOC -) (Arvidsson, 1998), reduced water-holding capacity/infiltration after a critical BD is reached (SOC +/-) (Archer & Smith, 1972; USDA Natural Resources Conservation Service, 2014), reduced microbial decomposition of OM through occlusion (SOC +) (Chenu et al., 2009), and/or root growth restrictions that limit plant biomass (SOC -) (Kozlowski, 1985; USDA Soil Quality Institute, 2003). Due to the complexities associated with BD, this metric cannot unravel the floodplain-specific SOC stock results.

4.3 Inundation as a predictor of SOC content with LTPBR

The initial inundation results reject my hypothesis since the areas inundated either frequently or infrequently exhibit the largest carbon stocks at LRV and LE. While the bimodal distribution was not observed at LBC, this was due to an absence of cores initially inundated at the lower recurrence interval discharges. Figure 16 provides an updated conceptual model based on the results from this study. It appears that the reasoning behind the hypothesis may be reversed to explain the results seen at LRV and LE. The areas inundated frequently may experience more frequent deposition of nutrient-rich sediments (Diehl et al., 2023) and the associated higher moisture content may support heightened plant primary productivity (Cooper & Merritt, 2012; Dwire et al., 2004). However, when studying the Difficult Run Watershed in Virginia, Hopkins et al. (2018) found that headwater stream floodplains primarily acted as a source of sediment from bank erosion rather than a sediment trap. Therefore, soil moisture likely plays a larger role in SOC storage in the frequently flooded areas. Areas inundated infrequently may still benefit from higher groundwater tables associated with floodplains that support plant growth that contributes to SOC content in the form of dead and decaying plant material that remains in these undisturbed areas (Lininger et al., 2018; Naiman & Décamps, 1997; Rieger et al., 2015; Scott & Wohl, 2018). Studies have shown significance for both lines of inference, making thoughtful site selection critical for increasing SOC storage through restoration (Bai et al., 2020; Gervais-Beaulac, 2013; Hupp et al., 2019; Saint-Laurent et al., 2014, 2016; Yin et al., 2019).

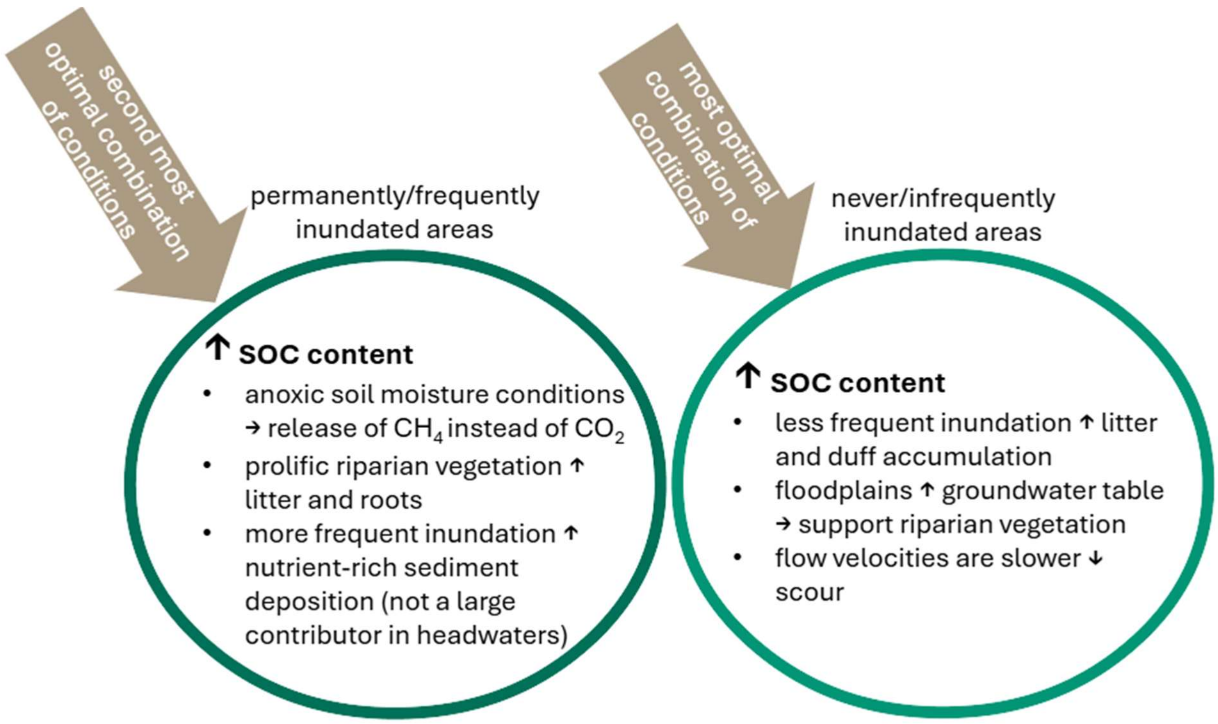

Figure 16. Updated conceptual model based on inundation and SOC results

LTPBR is known for being a cost-effective restoration strategy (American Rivers, 2022). Due to the low cost of implementation, it has become a common choice implemented across diverse riverine systems. I propose that a more thorough investigation of potential restoration sites be conducted prior to selection. Designers or project managers may not always have the luxury of selecting the restoration site. However, if the restoration goal is enhanced carbon sequestration for a carbon credit, I believe the floodplain and river system should be assessed to determine whether their characteristics (e.g., soil texture, historical presence of beaver dams or log jams, groundwater table, climate change impacts, hydrologic regime, etc.) would have the capacity to store more carbon.

4.4 Study Improvements

I have identified three areas that could improve this study to help refine the results and reduce the many sources of uncertainty.

4.4.1 Organic Layer Methods

The organic layer is composed of surficial plant litter, decomposing OM, and the root layer, making it temporally and spatially variable (Chapin et al., 2011; Kögel-Knabner, 2002; Sutfin & Wohl, 2017; Tufekcioglu et al., 2003). Sample collection timing, the presence of grazing animals, and current annual climate conditions could alter the composition of material collected as the organic layer. Therefore, the comparison of the organic layer samples among the three floodplains should be interpreted with caution.

In addition to the variability listed above, a subset of samples was tested for carbon content using both the EA and the LOI method. Comparison of methods for the LBC organic layer samples (n = 5) was provided by collaborators from RMRS. The percentage difference between the elemental analysis and LOI ranged from -46.37% to 3.71%. Organic layer methods comparison for LRV (n = 10) and LE (n = 10) was completed on samples I collected. The percentage differences between the two methodologies ranged from -86.59% to 4.24% and -19.74% to 17.70% for LRV and LE, respectively. The amount of variation between the two methods is large and inconsistent, suggesting that the LOI method may not be an accurate measure of carbon content.

An additional source of error was introduced by including the root layer as part of the organic layer. The root layer included mineral soils that were combusted with the collected OM. The removal of structural water from clay causes the conversion, using the van Bemmelen factor (0.58), from weight LOI to percent carbon to overestimate the sample's organic carbon content, reducing the accuracy of these results (Salehi et al., 2011; Sun et al., 2009; Tiller et al., 2025). In addition, a large number of studies have suggested the inappropriate use of a single-number conversion in accurately determining SOC content (Pribyl, 2010). Due to the amount of uncertainty associated with the organic layer, these data were not included in the results analysis.

4.4.2 Hydrodynamic Modeling

The hydrodynamic models simulated for this study utilize a steady-state model where discharge is held constant for the entire model run. A steady-state model was appropriate for the timeline and focus of this project. If time had permitted, the calculation and use of storm hydrographs for the various recurrence interval flows, necessary for an unsteady flow model, would have produced more realistic results (Van Der Steeg et al., 2023). Another benefit to an unsteady flow model is the ability to approximate inundation duration across the floodplain. The duration of inundation could inform whether the flood flows allow for groundwater percolation or sediment deposition through ponding and possibility of sediment erosion or plant scouring through continuous flow. Rain and flow gauges could be installed at these sites to create storm hydrographs for the studied floodplains. These data would make an unsteady flow model an achievable goal for the post-restoration comparison at these sites, especially if installed now.

4.4.3 Groundwater data

The importance of soil moisture in carbon storage and release has been written about in detail (Bai et al., 2020; Ise et al., 2008; Sutfin & Wohl, 2017). Pairing this study with quantitative groundwater data would enhance the results by providing the wetting extent and spatial and time components from various storm events. Groundwater data would also provide a better understanding of the rise and fall of the groundwater table, on annual and storm event time scales, which could influence microbial respiration and primary production. This information would help to parse out the influence of increased inundation area at lower flows and higher groundwater table elevations on floodplain SOC storage due to LTPBR structure installation. Again, the collection of groundwater data is an achievable goal for the post-restoration comparison at these sites, especially for LBC and LE as groundwater wells have already been installed.

Finally, the interactions on and within floodplain soils are extremely complex. Greater understanding at each floodplain seems to be integral in selecting a floodplain that has the ability to sequester additional carbon. The information collected and subsequent considerations must be made in the context of climate change. Climate is a complicated driver in floodplain SOC fluxes and especially for these headwater streams that are susceptible to climate change due to their reliance on contributions from snowmelt (Davidson & Janssens, 2006; Lee et al., 2015). Current flow regimes will be altered with a changing climate, which could cause shifts in current processes that regulate SOC storage in these complex and disturbance-adapted ecosystems.

5. CONCLUSION

Floodplains are complex systems shaped by hydrologic disturbance. Flooding introduces and distributes water, nutrient-rich sediments, and organic matter to the floodplain and influences the physical, biological, and chemical components collectively regulating the sequestration and release of carbon. This study identified a bimodal relationship between frequency of inundation and floodplain SOC storage, where both infrequently and frequently inundated areas exhibited elevated SOC content, whereas previous studies found that it was either the areas of frequent or infrequent inundation that corresponded with the highest floodplain SOC content. The lack of agreement between the studies highlights a broader uncertainty in floodplain SOC storage processes. To combat this uncertainty, continued research on the relationship between inundation dynamics and floodplain SOC storage should be completed on diverse river systems.

The goal of this study was to determine whether inundation frequency, commonly altered by the installation LTPBR structures, has a relationship with floodplain SOC storage. This information will help us to determine whether restoration to improve lateral connectivity is a viable carbon reduction project. The results show that floodplains differ in their capacity to store carbon and floodplain-specific characteristics strongly influence these outcomes, making a thorough pre-restoration site assessment of (at a minimum) groundwater dynamics, soil texture, and riparian vegetation integral. This additional work is feasible because of the relatively low installation cost of LTPBR structures. Additionally, this study provides a baseline dataset that can be leveraged in the future to quantify the magnitude and timeline of carbon sequestration or release following restoration in headwater floodplains.

6. REFERENCES

Addy, S., & Wilkinson, M. E. (2019). Representing natural and artificial in-channel large wood in numerical hydraulic and hydrological models. *WIREs Water*, *6*(6), e1389. https://doi.org/10.1002/wat2.1389

Aldridge, B. N., & Garrett, J. M. (1973). *Roughness Coefficients for Stream Channels in Arizona* (Open-File Report). Arizona Highway Department. Retrieved from https://pubs.usgs.gov/of/1973/0003/report.pdf

American Rivers. (2022). *Restoring Western Headwater Streams with Low-Tech Process-Vased Methods: A Review of the Science and Case Study Results, Challenges, and Opportunities* (White Paper).

Annala, M. J., Lehosmaa, K., Ahonen, S. H. K., Karttunen, K., Markkola, A. M., Puumala, I., & Mykrä, H. (2022). Effect of riparian soil moisture on bacterial, fungal and plant communities and microbial decomposition rates in boreal stream-side forests. *Forest Ecology and Management*, *519*, 120344. https://doi.org/10.1016/j.foreco.2022.120344

Appling, A. P., Bernhardt, E. S., & Stanford, J. A. (2014). Floodplain biogeochemical mosaics: A multidimensional view of alluvial soils: Floodplain biogeochemical mosaics. *Journal of Geophysical Research: Biogeosciences*, *119*(8), 1538–1553. https://doi.org/10.1002/2013JG002543

Aquaveo Staff. (2022, February 2). Understanding SRH-2D Obstructions [Blog Post]. Retrieved from https://aquaveo.com/blog/post/understanding-srh-2d-obstructions

Arcement, G. J., & Schneider, V. R. (1989). *Guide for Selecting Manning's Roughess Coefficients for Natural Channels and Flood Plains* (U.S. Geological Survey Water-

Supply Paper No. 2339). U.S. Department of Transportation, Federal Highway Administration. Retrieved from https://pubs.usgs.gov/wsp/2339/report.pdf

Archer, J. R., & Smith, P. D. (1972). THE RELATION BETWEEN BULK DENSITY, AVAILABLE WATER CAPACITY, AND AIR CAPACITY OF SOILS. *Journal of Soil Science*, *23*(4), 475–480. https://doi.org/10.1111/j.1365-2389.1972.tb01678.x

Arvidsson, J. (1998). Influence of soil texture and organic matter content on bulk density, air content, compression index and crop yield in field and laboratory compression experiments. *Soil and Tillage Research*, *49*(1–2), 159–170. https://doi.org/10.1016/S0167-1987(98)00164-0

Bai, J., Yu, L., Du, S., Wei, Z., Liu, Y., Zhang, L., et al. (2020). Effects of flooding frequencies on soil carbon and nitrogen stocks in river marginal wetlands in a ten-year period. *Journal of Environmental Management*, *267*, 110618. https://doi.org/10.1016/j.jenvman.2020.110618

Baker, B. W., & Hill, E. P. (2003). Beaver (Castor canadensis). In *Wild Mammals of North America: Biology, Management, and Conservation* (2nd ed., pp. 288–310). Baltimore, Maryland: The Johns Hopkins University Press.

Benjamini, Y., & Hochberg, Y. (1995). Controlling the False Discovery Rate: A Practical and Powerful Approach to Multiple Testing. *Journal of the Royal Statistical Society Series B: Statistical Methodology*, *57*(1), 289–300. https://doi.org/10.1111/j.2517-6161.1995.tb02031.x

Blazejewski, G. A., Stolt, M. H., Gold, A. J., & Groffman, P. M. (2005). Macro- and Micromorphology of Subsurface Carbon in Riparian Zone Soils. *Soil Science Society of America Journal*, *69*(4), 1320–1329. https://doi.org/10.2136/sssaj2004.0145

Bouwes, N., Weber, N., Jordan, C. E., Saunders, W. C., Tattam, I. A., Volk, C., et al. (2016). Ecosystem experiment reveals benefits of natural and simulated beaver dams to a threatened population of steelhead (Oncorhynchus mykiss). *Scientific Reports*, *6*(1), 28581. https://doi.org/10.1038/srep28581

Brazier, R. E., Puttock, A., Graham, H. A., Auster, R. E., Davies, K. H., & Brown, C. M. L. (2021). Beaver: Nature's ecosystem engineers. *WIREs Water*, *8*(1), e1494. https://doi.org/10.1002/wat2.1494

Brown, T. (2002). Floodplains, flooding, and salmon rearing habitats in British Columbia: A review. Fisheries and Oceans Canada Science. Retrieved from https://psf.ca/wp-content/uploads/2021/10/Download-PDF805-1.pdf

Bureau of Reclamation. (2024, August 5). SRH-2D: About SRH-2D. Retrieved January 16, 2026, from https://www.usbr.gov/tsc/techreferences/computer%20software/models/srh2d/index.html

Byrne, C. F., Stone, M. C., & Morrison, R. R. (2019). Scalable Flux Metrics at the Channel-Floodplain Interface as Indicators of Lateral Surface Connectivity During Flood Events. *Water Resources Research*, *55*(11), 9788–9807. https://doi.org/10.1029/2019WR026080

Cambardella, C. A., Gajda, A. M., Doran, J. W., Wienhold, B. J., & Kettler, T. A. (2000). Matter by Weight Loss-on-Ignition. In *Assessment methods for soil carbon* (p. 349).

Chapin, F. S., Matson, P. A., & Vitousek, P. M. (2011). *Principles of Terrestrial Ecosystem Ecology*. New York, NY: Springer New York. https://doi.org/10.1007/978-1-4419-9504-9

Cheng, B., Dai, H., Liu, T., Liu, H., Li, J., Qiao, R., et al. (2024). Mineralization characteristics of soil organic carbon under different herbaceous plant mosaics in semi-arid grasslands. *Scientific Reports*, *14*(1), 22196. https://doi.org/10.1038/s41598-024-73018-2

Chenu, C., Virto, I., Plante, A., & Elsass, F. (2009). Clay-Size Organo-Mineral Complexes in Temperate Soils: Relative Contributions of Sorptive and Physical Protection. In Y. Chen, C. Chenu, F. Elsass, J. M. Gonzalez, M. H. B. Hayes, D. A. Laird, et al., D. A. Laird, J. C. Silva, & D. A. Laird (Eds.), *Carbon Stabilization by Clays in the Environment* (pp. 119–135). Chantilly, VA: The Clay Minerals Society. https://doi.org/10.1346/CMS-WLS-16.6

Christensen, C., Nicholas. (2025). WRR submission 11-24 [Data set]. Hydraulic Model, HydroShare. Retrieved from http://www.hydroshare.org/resource/fb0150e68b4b4d388c7a7b26f0ffa9bb

Christensen, N., & Morrison, R. R. (2026). The Relative Importance of Floodplain Storage and Flow Path Dispersion on Flood Attenuation in Mountain Streams. *Water Resources Research*, *62*(1), e2024WR039628. https://doi.org/10.1029/2024WR039628

Chronic, J., & Chronic, H. (1972). *B-32 Prairie, Peak, and Plateau: A Guide to the Geology of Colorado*. Colorado Geological Survey. https://doi.org/10.58783/cgs.b32.sxdd4637

Cierjacks, A., Kleinschmit, B., Babinsky, M., Kleinschroth, F., Markert, A., Menzel, M., et al. (2010). Carbon stocks of soil and vegetation on Danubian floodplains. *Journal of Plant Nutrition and Soil Science*, *173*(5), 644–653. https://doi.org/10.1002/jpln.200900209

Colorado Water Conservation Board (CWCB). (2020). Colorado Statewide LiDAR dataset: Colorado Hazard Mapping & Risk MAP Portal [Data set]. LiDAR point cloud data. Retrieved from https://coloradohazardmapping.com/lidarDownload

Cooper, D. J., & Merritt, D. M. (2012). *Assessing the water needs of riparian and wetland vegetation in the western United States* (No. RMRS-GTR-282) (p. RMRS-GTR-282). Ft. Collins, CO: U.S. Department of Agriculture, Forest Service, Rocky Mountain Research Station. https://doi.org/10.2737/RMRS-GTR-282

Daugherty, E. E., McKee, G. A., Bergstrom, R., Burton, S., Pallud, C., Hubbard, R. M., et al. (2019). Hydrogeomorphic controls on soil carbon composition in two classes of subalpine wetlands. *Biogeochemistry*, *145*(1–2), 161–175. https://doi.org/10.1007/s10533-019-00597-y

Davidson, E. A., & Janssens, I. A. (2006). Temperature sensitivity of soil carbon decomposition and feedbacks to climate change. *Nature*, *440*(7081), 165–173. https://doi.org/10.1038/nature04514

De Vos, B., Vandecasteele, B., Deckers, J., & Muys, B. (2005). Capability of Loss-on-Ignition as a Predictor of Total Organic Carbon in Non-Calcareous Forest Soils. *Communications in Soil Science and Plant Analysis*, *36*(19–20), 2899–2921. https://doi.org/10.1080/00103620500306080

D'Elia, A. H., Liles, G. C., Viers, J. H., & Smart, D. R. (2017). Deep carbon storage potential of buried floodplain soils. *Scientific Reports*, *7*(1), 8181. https://doi.org/10.1038/s41598-017-06494-4

Diehl, R. M., Underwood, K. L., Triantafillou, S. P., Ross, D. S., Drago, S., & Wemple, B. C. (2023). Multi-scale drivers of spatial patterns in floodplain sediment and phosphorus deposition. *Earth Surface Processes and Landforms*, *48*(4), 801–816. https://doi.org/10.1002/esp.5519

Duan, H., Wang, L., Zhang, Y., Fu, X., Tsang, Y., Wu, J., & Le, Y. (2018). Variable decomposition of two plant litters and their effects on the carbon sequestration ability of wetland soil in the Yangtze River estuary. *Geoderma*, *319*, 230–238. https://doi.org/10.1016/j.geoderma.2017.10.050

Dwire, K. A., Kauffman, J. B., Brookshire, E. N. J., & Baham, J. E. (2004). Plant biomass and species composition along an environmental gradient in montane riparian meadows. *Oecologia*, *139*(2), 309–317. https://doi.org/10.1007/s00442-004-1498-2

Fisher, B., Turner, R. K., & Morling, P. (2009). Defining and classifying ecosystem services for decision making. *Ecological Economics*, *68*(3), 643–653. https://doi.org/10.1016/j.ecolecon.2008.09.014

Gee, G. W., & Bauder, J. W. (1986). Particle-size Analysis. In A. Klute (Ed.), *SSSA Book Series* (1st ed., Vol. 5, pp. 383–411). Wiley. https://doi.org/10.2136/sssabookser5.1.2ed.c15

Gervais-Beaulac, V. (2013). Organic carbon distribution in alluvial soils according to different flood risk zones. *Journal of Soil Science and Environmental Management*, *4*(8), 169–177. https://doi.org/10.5897/JSSEM13.0397

Gougoulias, C., Clark, J. M., & Shaw, L. J. (2014). The role of soil microbes in the global carbon cycle: tracking the below-ground microbial processing of plant-derived carbon for manipulating carbon dynamics in agricultural systems. *Journal of the Science of Food and Agriculture*, *94*(12), 2362–2371. https://doi.org/10.1002/jsfa.6577

Graf-Rosenfellner, M., Cierjacks, A., Kleinschmit, B., & Lang, F. (2016). Soil formation and its implications for stabilization of soil organic matter in the riparian zone. *CATENA*, *139*, 9–18. https://doi.org/10.1016/j.catena.2015.11.010

Gurwick, N. P., Groffman, P. M., Yavitt, J. B., Gold, A. J., Blazejewski, G., & Stolt, M. (2008). Microbially available carbon in buried riparian soils in a glaciated landscape. *Soil Biology and Biochemistry*, *40*(1), 85–96. https://doi.org/10.1016/j.soilbio.2007.07.007

Hahn, A., Morrison, R. R., Triantafillou, S., & Wohl, E. (In Review). Predicting Head Loss and Hydraulic Roughness of Channel-Spanning Large Wood Jams.

Hahn, A. J., Christensen, N. D., White, D. C., Wohl, E., & Morrison, R. R. (2025). Trajectories of river-floodplain morphology and hydraulics following compounding wildfire-flood disturbances. *Earth Surface Processes and Landforms*, *50*(5), e70057. https://doi.org/10.1002/esp.70057

Hallberg, L., Larsen, A., Ceperley, N., d'Epagnier, R., Brouwers, T. F., Schaefli, B., et al. (2026). Beavers can convert stream corridors to persistent carbon sinks. *Communications Earth & Environment*, *7*(1), 227. https://doi.org/10.1038/s43247-026-03283-8

Hassink, J., & Whitmore, A. P. (1997). A Model of the Physical Protection of Organic Matter in Soils. *Soil Science Society of America Journal*, *61*(1), 131–139. https://doi.org/10.2136/sssaj1997.03615995006100010020x

Heger, A., Becker, J. N., Vásconez Navas, L. K., & Eschenbach, A. (2021). Factors controlling soil organic carbon stocks in hardwood floodplain forests of the lower middle Elbe River. *Geoderma*, *404*, 115389. https://doi.org/10.1016/j.geoderma.2021.115389

Hinshaw, S., & Wohl, E. (2023). Carbon sequestration potential of process-based river restoration. *River Research and Applications*, *39*(9), 1812–1827. https://doi.org/10.1002/rra.4183

Hopkins, K. G., Noe, G. B., Franco, F., Pindilli, E. J., Gordon, S., Metes, M. J., et al. (2018). A method to quantify and value floodplain sediment and nutrient retention ecosystem services. *Journal of Environmental Management*, *220*, 65–76. https://doi.org/10.1016/j.jenvman.2018.05.013

Hunt, B. (1990). An Approximation for the Bank Storage Effect. *Water Resources Research*, *26*(11), 2769–2775. https://doi.org/10.1029/WR026i011p02769

Hunt, L. J. H., Fair, J., & Odland, M. (2018). Meadow Restoration Increases Baseflow and Groundwater Storage in the Sierra Nevada Mountains of California. *JAWRA Journal of the American Water Resources Association*, *54*(5), 1127–1136. https://doi.org/10.1111/1752-1688.12675

Hupp, C. R., Kroes, D. E., Noe, G. B., Schenk, E. R., & Day, R. H. (2019). Sediment Trapping and Carbon Sequestration in Floodplains of the Lower Atchafalaya Basin, LA: Allochthonous Versus Autochthonous Carbon Sources. *Journal of Geophysical Research: Biogeosciences*, *124*(3), 663–677. https://doi.org/10.1029/2018JG004533

Intergovernmental Panel On Climate Change (Ipcc). (2023). *Climate Change 2021 – The Physical Science Basis: Working Group I Contribution to the Sixth Assessment Report of the Intergovernmental Panel on Climate Change* (1st ed.). Cambridge University Press. https://doi.org/10.1017/9781009157896

Iqbal, J., Thomasson, J. A., Jenkins, J. N., Owens, P. R., & Whisler, F. D. (2005). Spatial Variability Analysis of Soil Physical Properties of Alluvial Soils. *Soil Science Society of America Journal*, *69*(4), 1338–1350. https://doi.org/10.2136/sssaj2004.0154

Ise, T., Dunn, A. L., Wofsy, S. C., & Moorcroft, P. R. (2008). High sensitivity of peat decomposition to climate change through water-table feedback. *Nature Geoscience*, *1*(11), 763–766. https://doi.org/10.1038/ngeo331

ISO. (1995). Soil quality - Determination of organic and total carbon after dry combustion (elementary analysis). ISO.

Jobbágy, E. G., & Jackson, R. B. (2000). THE VERTICAL DISTRIBUTION OF SOIL ORGANIC CARBON AND ITS RELATION TO CLIMATE AND VEGETATION. *Ecological Applications*, *10*(2), 423–436. https://doi.org/10.1890/1051-0761(2000)010%5B0423:TVDOSO%5D2.0.CO;2

Johnson, K. L., Barnett, L. O., Gunay, F., Hess, J. P., Krygier, J. T., Lee, R., et al. (1963). *Watershed Analysis of the Little South Fork of the Cache la Poudre River*. Cooperative Watershed Management Unit Colorado State University. Retrieved from https://mountainscholar.org/bitstreams/92e67d30-2ddb-4cfb-a388-19220d37eee0/download

Jones, H., Kelleher, C., & Shaw, S. B. (2026). Assessing the Effects of Beaver Dam Analogues on Valley Bottom and Watershed Storage at a Site in Central Wyoming. *Hydrological Processes*, *40*(1), e70381. https://doi.org/10.1002/hyp.70381

Junk, W. J., Bayley, P. B., & Sparks, R. E. (1989). The Flood Pulse Concept in River-Floodplain Systems.

Knox, R. L., Wohl, E. E., & Morrison, R. R. (2022). Levees don't protect, they disconnect: A critical review of how artificial levees impact floodplain functions. *Science of The Total Environment*, *837*, 155773. https://doi.org/10.1016/j.scitotenv.2022.155773

Kögel-Knabner, I. (2002). The macromolecular organic composition of plant and microbial residues as inputs to soil organic matter. *Soil Biology and Biochemistry*, *34*(2), 139–162. https://doi.org/10.1016/S0038-0717(01)00158-4

Kozlowski, T. T. (1985). Soil Aeration, Flooding, and Tree Growth. *Arboriculture & Urban Forestry*, *11*(3), 85–95. https://doi.org/10.48044/jauf.1985.022

Kruskal, W. H., & Wallis, W. A. (1952). Use of Ranks in One-Criterion Variance Analysis. *Journal of the American Statistical Association*, *47*(260), 583–621. https://doi.org/10.1080/01621459.1952.10483441

Ladd, C. J. T., Smeaton, C., Skov, M. W., & Austin, W. E. N. (2022). Best practice for upscaling soil organic carbon stocks in salt marshes. *Geoderma*, *428*, 116188. https://doi.org/10.1016/j.geoderma.2022.116188

Lal, R. (2008). Carbon sequestration. *Philosophical Transactions of the Royal Society B: Biological Sciences*, *363*(1492), 815–830. https://doi.org/10.1098/rstb.2007.2185

Lang, A. K., Pastore, M. A., Walters, B. F., & Domke, G. M. (2025). Bulk density calculation methods systematically alter estimates of soil organic carbon stocks in United States forests. *Biogeochemistry*, *168*(3), 44. https://doi.org/10.1007/s10533-025-01235-6

Larsen, A., Larsen, J. R., & Lane, S. N. (2021). Dam builders and their works: Beaver influences on the structure and function of river corridor hydrology, geomorphology, biogeochemistry and ecosystems. *Earth-Science Reviews*, *218*, 103623. https://doi.org/10.1016/j.earscirev.2021.103623

Lee, S.-Y., Ryan, M. E., Hamlet, A. F., Palen, W. J., Lawler, J. J., & Halabisky, M. (2015). Projecting the Hydrologic Impacts of Climate Change on Montane Wetlands. *PLOS ONE*, *10*(9), e0136385. https://doi.org/10.1371/journal.pone.0136385

Limerinos, J. T. (1970). *Determination of the manning coefficient from measured bed roughness in natural channels*. https://doi.org/10.3133/wsp1898B

Lininger, K. B., Wohl, E., & Rose, J. R. (2018). Geomorphic Controls on Floodplain Soil Organic Carbon in the Yukon Flats, Interior Alaska, From Reach to River Basin Scales. *Water Resources Research*, *54*(3), 1934–1951. https://doi.org/10.1002/2017WR022042

Lininger, K. B., Wohl, E., Rose, J. R., & Leisz, S. J. (2019). Significant Floodplain Soil Organic Carbon Storage Along a Large High-Latitude River and its Tributaries. *Geophysical Research Letters*, *46*(4), 2121–2129. https://doi.org/10.1029/2018GL080996

Lininger, Katherine B, & Lave, R. (2024). River restoration can increase carbon storage but is not yet a suitable basis for carbon credits. *BioScience*, *74*(10), 717–724. https://doi.org/10.1093/biosci/biae083

Lininger, Katherine B., & Polvi, L. E. (2020). Evaluating floodplain organic carbon across a gradient of human alteration in the boreal zone. *Geomorphology*, *370*, 107390. https://doi.org/10.1016/j.geomorph.2020.107390

Mahoney, J. M., & Rood, S. B. (1998). Streamflow requirements for cottonwood seedling recruitment—An integrative model. *Wetlands*, *18*(4), 634–645. https://doi.org/10.1007/BF03161678

Matzek, V., Puleston, C., & Gunn, J. (2015). Can carbon credits fund riparian forest restoration? *Restoration Ecology*, *23*(1), 7–14. https://doi.org/10.1111/rec.12153

Merritt, D. M., Scott, M. L., LeROY Poff, N., Auble, G. T., & Lytle, D. A. (2010). Theory, methods and tools for determining environmental flows for riparian vegetation: riparian vegetation-flow response guilds. *Freshwater Biology*, *55*(1), 206–225. https://doi.org/10.1111/j.1365-2427.2009.02206.x

Milford, M. (2010). *Introduction to soils and soil science: laboratory exercises*. Place of publication not identified: Kendall Hunt.

Morrison, R. R., Simonson, K., McManamay, R. A., & Carver, D. (2023). Degradation of floodplain integrity within the contiguous United States. *Communications Earth & Environment*, *4*(1), 215. https://doi.org/10.1038/s43247-023-00877-4

Naiman, R. J., & Décamps, H. (1997). The Ecology of Interfaces: Riparian Zones. *Annual Review of Ecology and Systematics*, *28*(1), 621–658. https://doi.org/10.1146/annurev.ecolsys.28.1.621

Nanson, G. C., & Croke, J. C. (1992). A genetic classification of floodplains. *Geomorphology*, *4*(6), 459–486. https://doi.org/10.1016/0169-555X(92)90039-Q

National Geodetic Survey. (2025a). User Friendly CORS (UFCORS). Retrieved from https://geodesy.noaa.gov/UFCORS/

National Geodetic Survey. (2025b, November 17). OPUS: Online Positioning User Service [Governmental]. Retrieved from https://geodesy.noaa.gov/OPUS/

Pinay, G., Fabre, A., Vervier, Ph., & Gazelle, F. (1992). Control of C,N,P distribution in soils of riparian forests. *Landscape Ecology*, *6*(3). https://doi.org/10.1007/BF00130025

Poff, N. L., Allan, J. D., Bain, M. B., Karr, J. R., Prestegaard, K. L., Richter, B. D., et al. (1997). The Natural Flow Regime. *BioScience*, *47*(11), 769–784. https://doi.org/10.2307/1313099

Pribyl, D. W. (2010). A critical review of the conventional SOC to SOM conversion factor. *Geoderma*, *156*(3–4), 75–83. https://doi.org/10.1016/j.geoderma.2010.02.003

Reed, C. C., Berhe, A. A., Moreland, K. C., Wilcox, J., & Sullivan, B. W. (2022). Restoring function: Positive responses of carbon and nitrogen to 20 years of hydrologic restoration in montane meadows. *Ecological Applications*, *32*(7), e2677. https://doi.org/10.1002/eap.2677

Rieger, I., Kowarik, I., & Cierjacks, A. (2015). Drivers of carbon sequestration by biomass compartment of riparian forests. *Ecosphere*, *6*(10), 1–16. https://doi.org/10.1890/ES14-00330.1

Rodrigues, C. I. D., Brito, L. M., & Nunes, L. J. R. (2023). Soil Carbon Sequestration in the Context of Climate Change Mitigation: A Review. *Soil Systems*, *7*(3), 64. https://doi.org/10.3390/soilsystems7030064

Ruffing, C. M., Dwire, K. A., & Daniels, M. D. (2016). Carbon pools in stream-riparian corridors: legacy of disturbance along mountain streams of south-eastern Wyoming. *Earth Surface Processes and Landforms*, *41*(2), 208–223. https://doi.org/10.1002/esp.3830

Saint-Laurent, D., Beaulac-Gervais, V., & Berthelot, J. S. (2014). Comparison of soil organic carbon and total nitrogen contents in inundated and non-inundated zones in southern Québec, Canada. *CATENA*, *113*, 1–8. https://doi.org/10.1016/j.catena.2013.09.005

Saint-Laurent, D., Paradis, R., Drouin, A., & Gervais-Beaulac, V. (2016). Impacts of Floods on Organic Carbon Concentrations in Alluvial Soils along Hydrological Gradients Using a Digital Elevation Model (DEM). *Water*, *8*(5), 208. https://doi.org/10.3390/w8050208

Salehi, M. H., Beni, O. H., Harchegani, H. B., Borujeni, I. E., & Motaghian, H. R. (2011). Refining Soil Organic Matter Determination by Loss-on-Ignition. *Pedosphere*, *21*(4), 473–482. https://doi.org/10.1016/S1002-0160(11)60149-5

Schimel, D. S., House, J. I., Hibbard, K. A., Bousquet, P., Ciais, P., Peylin, P., et al. (2001). Recent patterns and mechanisms of carbon exchange by terrestrial ecosystems. *Nature*, *414*(6860), 169–172. https://doi.org/10.1038/35102500

Schmudde, T. H. (1968). Flood plain. In *Geomorphology* (pp. 359–362). Springer, Berlin, Heidelberg. https://doi.org/10.1007/3-540-31060-6_131

Schultz, K., Morrison, R., Rathburn, S., & Nelson, P. (2025). Loss of beaver dams decreases floodplain connectivity in Colorado headwater streams [Born digital,masters theses]. Colorado State University. Libraries. https://doi.org/10.25675/3.02085

Scott, D. N., & Wohl, E. E. (2018). Geomorphic regulation of floodplain soil organic carbon concentration in watersheds of the Rocky and Cascade Mountains, USA. *Earth Surface Dynamics*, *6*(4), 1101–1114. https://doi.org/10.5194/esurf-6-1101-2018

Shapiro, S. S., & Wilk, M. B. (1965). An Analysis of Variance Test for Normality (Complete Samples). *Biometrika*, *52*(3/4), 591. https://doi.org/10.2307/2333709

Smith, S. D., Wellington, A. B., Nachlinger, J. L., & Fox, C. A. (1991). Functional Responses of Riparian Vegetation to Streamflow Diversion in the Eastern Sierra Nevada. *Ecological Applications*, *1*(1), 89–97. https://doi.org/10.2307/1941850

Sufian, O. (2021). Adsorption: An Important Phenomenon in Controlling Soil Properties and Carbon Stabilization. In R. Datta & R. S. Meena (Eds.), *Soil Carbon Stabilization to Mitigate Climate Change* (pp. 205–241). Singapore: Springer Singapore. https://doi.org/10.1007/978-981-33-6765-4_6

Sun, H., Nelson, M., Chen, F., & Husch, J. (2009). Soil mineral structural water loss during loss on ignition analyses. *Canadian Journal of Soil Science*, *89*(5), 603–610. https://doi.org/10.4141/CJSS09007

Sutfin, N. A., & Wohl, E. (2017). Substantial soil organic carbon retention along floodplains of mountain streams. *Journal of Geophysical Research: Earth Surface*, *122*(7), 1325–1338. https://doi.org/10.1002/2016JF004004

Sutfin, N. A., Wohl, E. E., & Dwire, K. A. (2016). Banking carbon: a review of organic carbon storage and physical factors influencing retention in floodplains and riparian ecosystems. *Earth Surface Processes and Landforms*, *41*(1), 38–60. https://doi.org/10.1002/esp.3857

Sutfin, N. A., Wohl, E., Fegel, T., Day, N., & Lynch, L. (2021). Logjams and Channel Morphology Influence Sediment Storage, Transformation of Organic Matter, and Carbon Storage Within Mountain Stream Corridors. *Water Resources Research*, *57*(5), e2020WR028046. https://doi.org/10.1029/2020WR028046

Throop, H. L., Archer, S. R., Monger, H. C., & Waltman, S. (2012). When bulk density methods matter: Implications for estimating soil organic carbon pools in rocky soils. *Journal of Arid Environments*, *77*, 66–71. https://doi.org/10.1016/j.jaridenv.2011.08.020

Tiller, M., Reading, L., Dawes, L., Miska, M., & Egodawatta, P. (2025). Effects of particle size fractions and clay content for determination of soil organic carbon and soil organic matter. *Soil and Tillage Research*, *252*, 106568. https://doi.org/10.1016/j.still.2025.106568

Tisdall, J. M., & Oades, J. M. (1982). Organic matter and water-stable aggregates in soils. *Journal of Soil Science*, *33*(2), 141–163. https://doi.org/10.1111/j.1365-2389.1982.tb01755.x

Tockner, K., & Stanford, J. A. (2002). Riverine flood plains: present state and future trends. *Environmental Conservation*, *29*(3), 308–330. https://doi.org/10.1017/S037689290200022X

Tufekcioglu, A., Raich, J. W., Isenhart, T. M., & Schultz, R. C. (2003). Biomass, carbon and nitrogen dynamics of multi-species riparian buffers within an agricultural watershed in

Iowa, USA. *Agroforestry Systems*, *57*(3), 187–198. https://doi.org/10.1023/A:1024898615284

U.S. Geological Survey. (2019). The StreamStats program. Retrieved from https://streamstats.usgs.gov/ss

USDA Natural Resources Conservation Service. (2014). *Soil Infiltration* (Soil Health - Guides for Educators). Retrieved from https://www.nrcs.usda.gov/sites/default/files/2022-10/Soil%20Infiltration.pdf#:~:text=Compacted%20or%20impervious%20soil%20layers%20have%20less,restricts%20water%20movement%20through%20the%20soil%20profile.

USDA Natural Resources Conservation Service. (2019, July 31). Web Soil Survey [Governmental]. Retrieved from https://websoilsurvey.nrcs.usda.gov/app/

USDA Natural Resources Conservation Service. (2026, March 9). AWS Plot - Joe Wright, CO (551) Precipitation Accumulation [Governmental]. Retrieved from https://nwcc-apps.sc.egov.usda.gov/awdb/site-plots/POR/PREC/CO/Joe%20Wright.html

USDA Soil Quality Institute. (2001). *Soil Quality Test Kit Guide*. Washington, D.C.: USDA.

USDA Soil Quality Institute. (2003). *Soil Compaction: Detection, Prevention, and Alleviation* (Agronomy Technical Note No. 17).

Van Der Steeg, S., Torres, R., Viparelli, E., Xu, H., Elias, E., & Sullivan, J. C. (2023). Floodplain Surface-Water Circulation Dynamics: Congaree River, South Carolina, USA. *Water Resources Research*, *59*(1), e2022WR032982. https://doi.org/10.1029/2022WR032982

Walling, D. E., & He, Q. (1998). The spatial variability of overbank sedimentation on river floodplains. *Geomorphology*, *24*(2–3), 209–223. https://doi.org/10.1016/S0169-555X(98)00017-8

WECo. (2026). Colorado Aquifers [Organization]. Retrieved from https://watereducationcolorado.org/water-101/hydrology-water-resources/colorado-aquifers/

Whiting, P. J., & Pomeranets, M. (1997). A numerical study of bank storage and its contribution to streamflow. *Journal of Hydrology*, *202*(1–4), 121–136. https://doi.org/10.1016/S0022-1694(97)00064-4

Wilcoxon, F. (1945). Individual Comparisons by Ranking Methods. *Biometrics Bulletin*, *1*(6), 80. https://doi.org/10.2307/3001968

Wohl, E. (2021). An Integrative Conceptualization of Floodplain Storage. *Reviews of Geophysics*, *59*(2), e2020RG000724. https://doi.org/10.1029/2020RG000724

Wohl, E., & Knox, R. L. (2022). A first-order approximation of floodplain soil organic carbon stocks in a river network: The South Platte River, Colorado, USA as a case study. *Science of The Total Environment*, *852*, 158507. https://doi.org/10.1016/j.scitotenv.2022.158507

Wohl, E., Dwire, K., Sutfin, N., Polvi, L., & Bazan, R. (2012). Mechanisms of carbon storage in mountainous headwater rivers. *Nature Communications*, *3*(1), 1263. https://doi.org/10.1038/ncomms2274

Wohl, E., Hall, R. O., Lininger, K. B., Sutfin, N. A., & Walters, D. M. (2017). Carbon dynamics of river corridors and the effects of human alterations. *Ecological Monographs*, *87*(3), 379–409. https://doi.org/10.1002/ecm.1261

Wohl, E., Scott, D., & Yochum, S. (2019). *Managing for large wood and beaver dams in stream corridors* (General Technical Report No. RMRS-GTR-404). Rocky Mountain Research Station.

Woltemade, C. J., & Potter, K. W. (1994). A watershed modeling analysis of fluvial geomorphologic influences on flood peak attenuation. *Water Resources Research*, *30*(6), 1933–1942. https://doi.org/10.1029/94WR00323

Wright, A. J., Ebeling, A., De Kroon, H., Roscher, C., Weigelt, A., Buchmann, N., et al. (2015). Flooding disturbances increase resource availability and productivity but reduce stability in diverse plant communities. *Nature Communications*, *6*(1), 6092. https://doi.org/10.1038/ncomms7092

Yin, S., Bai, J., Wang, W., Zhang, G., Jia, J., Cui, B., & Liu, X. (2019). Effects of soil moisture on carbon mineralization in floodplain wetlands with different flooding frequencies. *Journal of Hydrology*, *574*, 1074–1084. https://doi.org/10.1016/j.jhydrol.2019.05.007

7. APPENDICES

7.1 Appendix A: Applicable Lab and Field Information

Two samples of the 638 collected were not processed. One sample LE_T4_E125_L3_3-21 (LEM26) was assigned to be processed for texture, but due to the total mass of the sample (< 50 g) the protocol could not be completed. The second sample that was not processed was LE_T2_E125_L2_8.5-21 (LEM94). The entire sample was comprised of a root, with an insufficient amount of soil mass available for EA.

Due to a technical issue the data for the initial drying and weighing of the organic layer samples listed in Table 11 were lost. However, the drying process had been completed prior to the loss of data. There was a less than 1% change in weight between October 22, 2025, at ~ 9:30 am MT to October 23, 2025, at ~ 7:25 am MT.

Table 11. List of LRV organic layer cores that lost initial drying and weight data

Field Sample Name	Lab Sample Name
LRV_T1_E00_L4_0-3.2	LRVO4
LRV_T2_E125_L1_0-2.7	LRVO9
LRV_T4_E125_L4_0-3.1	LRVO19
LRV_T4_E10_L7_0-3.3	LRVO22
LRV_T3_E025_L1_0-4.5	LRVO23
LRV_T4_E05_L8_0-2.6	LRVO28
LRV_T5_E10_L8_0-4.5	LRVO37
LRV_T8_E00_L2_0-1.2	LRVO39
LRV_T6_E025_L5_0-4.3	LRVO47
LRV_T7_E075_L5_0-3	LRVO54

Table 12. Core location GPS errors

Field Core ID	Relative Elevation (m)	Final Elevation Bin (based on GIS relative elevation)	Updated Core ID
LBC_T1_E050_L1	0.41	0.25-0.5	LBC_T1_E025_L1
LBC_T1_E050_L2	0.38	0.25-0.5	LBC_T1_E025_L2
LBC_T1_E050_L3	0.49	0.25-0.5	LBC_T1_E025_L3
LBC_T1_E050_L4	0.45	0.25-0.5	LBC_T1_E025_L4
LBC_T2_E100_L1	0.56	0.5-0.75	LBC_T2_E050_L1
LBC_T2_E050_L2	0.35	0.25-0.5	LBC_T2_ E025_L2
LBC_T3_E075_L5	0.54	0.5-0.75	LBC_T3_ E050_L5
LBC_T4_E075_L1	0.75	0.5-0.75	LBC_T4_ E050_L1
LBC_T4_E050_L6	0.76	0.75-1.0	LBC_T4_ E075_L6
LBC_T5_E125_L1	1.22	1.0-1.25	LBC_T5_ E100_L1
LBC_T5_E125_L2	1.16	1.0-1.25	LBC_T5_E100_L2
LBC_T5_E000_L7	0.25	0.25-0.5	LBC_T5_ E025_L7
LBC_T6_E125_L1	0.94	0.75-1.0	LBC_T6_E075_L1
LRV_T1_E000_L1	0.26	0.25-0.5	LRV_T1_E025_L1
LRV_T1_E050_L6	0.77	0.75-1.0	LRV_T1_E075_L6
LRV_T2_E075_L6	0.64	0.5-0.75	LRV_T2_E050_L6
LRV_T4_E075_L5	1.03	1.0-1.25	LRV_T4_E100_L5
LRV_T3_E000_L4	0.34	0.25-0.5	LRV_T3_E025_L4
LRV_T3_E050_L5	0.82	0.75-1.0	LRV_T3_E075_L5
LRV_T4_E050_L8	1.04	1.0-1.25	LRV_T4_E100_L8
LRV_T4_E025_L9	0.67	0.5-0.75	LRV_T4_E050_L9
LRV_T5_E075_L1	1.01	1.0-1.25	LRV_T5_E100_L1
LRV_T5_E125_L3	1.17	1.0-1.25	LRV_T5_E100_L3
LRV_T8_E075_L4	0.65	0.5-0.75	LRV_T8_E050_L4
LRV_T6_E025_L5	0.58	0.5-0.75	LRV_T6_E050_L5
LE_T1_E125_L2	1.16	1.0-1.25	LE_T1_E100_L2
LE_T2_E075_L3	0.58	0.5-0.75	LE_T2_E050_L3
LE_T6_E075_L1	0.51	0.5-0.75	LE_T6_E050_L1
LE_T6_E050_L2	0.32	0.25-0.5	LE_T6_E025_L2
LE_T6_E075_L3	0.71	0.5-0.75	LE_T6_E050_L3
LE_T5_E050_L6	0.45	0.25-0.5	LE_T5_E025_L6

Table 13. Example field notes from a core collected at LBC

LBC_T5_E125_L1			
Probe Depth: >1 m			
Depth (cm)	**Organic/Mineral**	**Dimensions (cm)**	**Notes**
0-0.4	O	13.7x14	Dead and decomposing grasses with small amount of roots.
0.4-18.9	M	--	Fine roots throughout holding together soil aggregates. Light brown fine sand.
18.9-30.4	M	--	~ 3 cm of compaction. Left, ~5 cm in hole. Dry crumbly texture (fine sand soil aggregates). Fine roots present and a few medium.
30.4-52.5	M	--	Light brown sandy core, very few roots.
52.5-70.4	M	--	Medium brown not cohesive soil with oxidation present. Few fine roots.
70.4-80.9	M	--	Sandy brown, grey soil with some oxidation. Few fine roots. Hit gravel layer/rock.

7.2 Appendix B: Manning's *n* Calibration and Validation

Table 14. LBC, LRV, and LE's channel Manning's *n* initial estimation

	Channel *n*-value	Justification	Floodplain *n*-value	Justification
			LBC	
n_b	--	--	0.025	Firm soil
n_1	--	--	0.005	Some variation in topography close to the channel, but overall, relatively consistent
n_2	--	--	NA	Not applicable for floodplains
n_3	--	--	0.012	Few obstructions on channel left, while there were many on channel right
n_4	--	--	0.0375	Mature willows, but sparsely spaced. Shorter grasses further up the floodplain
m	--	--	NA	
n	**0.04** (N. Christensen & Morrison, 2026)			**0.0795**
			LRV	
n_b	0.03	Cobbles and coarse gravel make up channel bed	0.03	Firm soil
n_1	0.02	Severe sloughing and channel bank erosion	0.02	Floodplain is very irregular, many depressions and side channels
n_2	0.0025	Cross-section size and flow (laterally) alternates occasionally	NA	Not applicable for floodplains
n_3	0.0175	Obstructions widely spaced longitudinally, but channel spanning	0.019	Downed trees and forested areas near upstream and downstream extents. Few obstructions in open floodplain area.
n_4	0.015	Willows growing along the bank, little vegetation within channel	0.15	Coniferous forests at upstream and downstream extents. Dense willows along throughout middle floodplain area
m	1.15	Ratio of channel length to valley length is between 1.2-1.5	NA	Not applicable for floodplains
n	**0.098**			**0.219**
			LE	
n_b	0.03	Cobbles and coarse gravel make up channel bed	0.03	Firm soil
n_1	0.008	Largely stable channel banks with areas severe bank erosion	0.02	Floodplain is very irregular, many depressions, side channels, and standing water areas
n_2	0.0025	Cross-section size is relatively consistent, but flow (laterally) alternates frequently	NA	Not applicable for floodplains
n_3	0.015	Obstructions partially spanning channel are widely spaced longitudinally	0.01	Areas of elevated topography and areas of accumulated woody debris

n_4	0.01	Willows and dense grasses growing along the bank, little vegetation within channel	0.1	Dense and tall grasses on open area of floodplain with scattered willows along channel banks
m	1.15	Ratio of channel length to valley length is between 1.2-1.5	NA	Not applicable for floodplains
n		**0.075**		**0.16**

Table 15. LRV channel Manning's *n* calibration log

Channel *n*-value	Beaver Dam *n*-value	Floodplain *n*-value	ME	RMSE	ME**	RMSE**
0.098	NA	0.219	-0.014	0.139	0.016	0.083
0.095	*NA*	*0.219*	*-0.017*	*0.138*	*0.012*	*0.081*
0.09	NA	0.219	-0.025	0.141	0.006	0.08
0.08	NA	0.219	-0.041	0.144	-0.011	0.079
0.075	NA	0.219	-0.05	0.147	-0.02	0.082
0.085	NA	0.219	-0.033	0.142	-0.03	0.08
0.105	NA	0.219	-0.004	0.139	0.026	0.086
0.08	2.0	0.219	-0.032	0.132	-0.011	0.081
0.08	2.5	0.219	-0.032	0.132	-0.011	0.081
0.095	**2.5**	**0.219**	**-0.011 | -0.007***	**0.128 | 0.126***	**0.011 | 0.019***	**0.082 | 0.080***
0.01	2.5	0.219	-0.004	0.0129	0.018	0.084

*Statistical values computed manually. All other ME and RMSE were calculated in SRH-2D.
**Dam affected observation points were removed from the ME and RMSE calculations

Table 16. LE channel Manning's *n* calibration log

Channel *n*-value		Floodplain *n*-value	ME	RMSE
0.075		0.16	-0.048	0.144
0.07		0.16	-0.054	0.146
0.09		0.16	-0.027	0.133
0.1		0.16	-0.013	0.128
0.11		*0.16*	*0.000*	*0.128*
0.115		0.16	0.005	0.128
0.105		0.16	-0.006	0.128
US	**DS**			
0.06	0.135	0.16	-0.01	0.115
0.065	0.135	0.16	-0.011	0.115
0.065	0.14	0.16	-0.008 | 0.0038*	0.114 | 0.104*
0.06	**0.14**	**0.16**	**-0.008 | 0.001***	**0.114 | 0.103***

*Statistical values computed manually. All other ME and RMSE were calculated in SRH-2D.

7.3 Appendix C: Statistical Normality Data

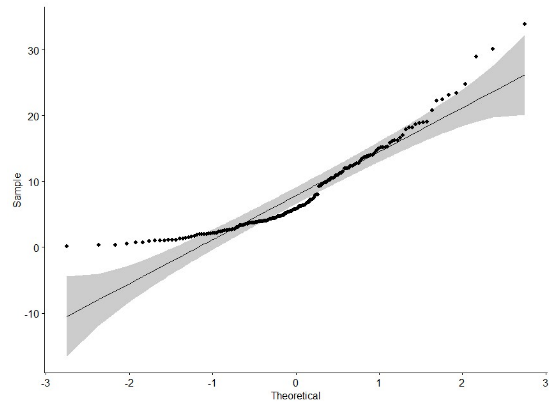

Figure 17. LBC qq-plot testing percent carbon normality (all samples)

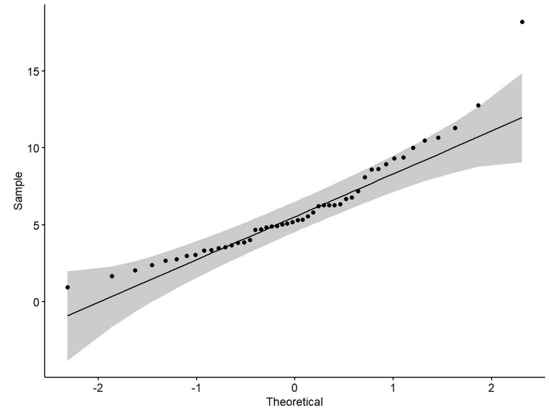

Figure 18. LBC qq-plot testing percent carbon normality (depth-averaged percent carbon per core location)

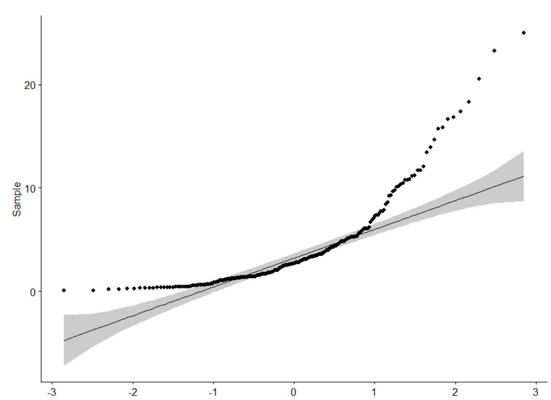

Figure 19. LRV qq-plot testing percent carbon normality (all samples)

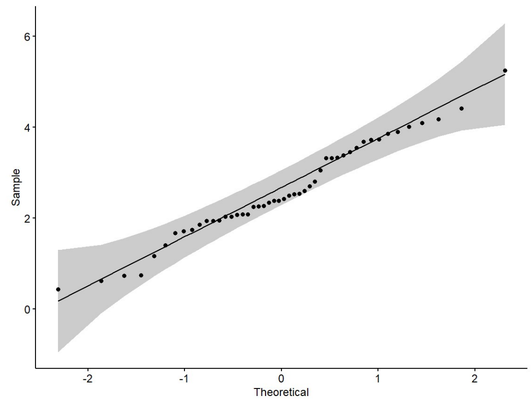

Figure 20. LRV qq-plot testing percent carbon normality (depth-averaged percent carbon per core location)

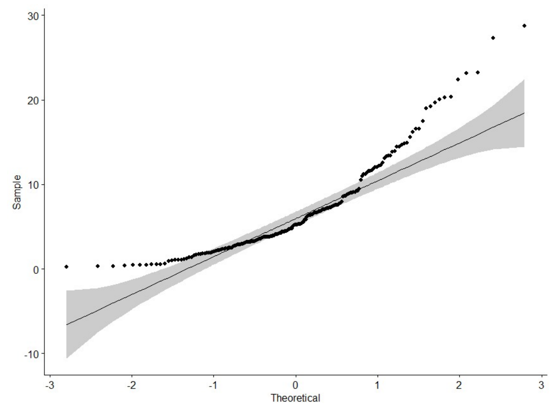

Figure 21. LE qq-plot testing percent carbon normality (all samples)

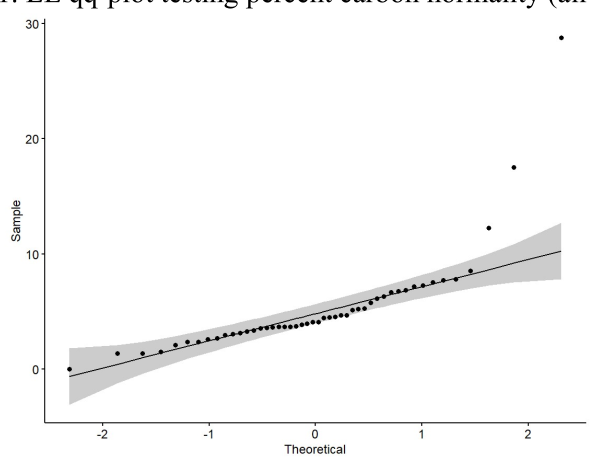

Figure 22. LE qq-plot testing percent carbon normality (depth-averaged percent carbon per core location)

7.4 Appendix D: Relationship between Volume Averaged Percent Carbon and Relative Surface Elevation Above the Channel

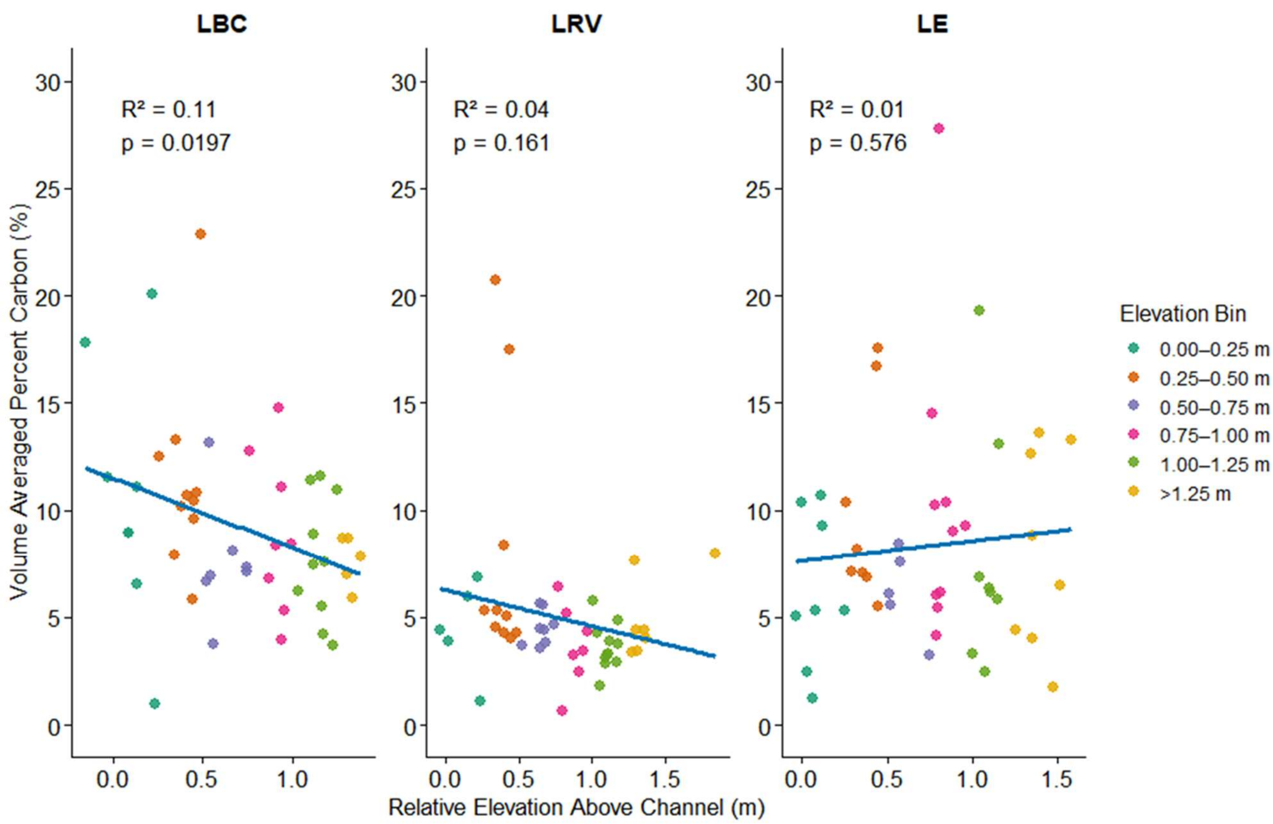

Figure 23. Volume-averaged percent carbon against relative surface elevation above the channel for the LBC, LRV, and LE floodplains

7.5 Appendix E: Total Bulk Density Active Layer Organic Carbon Stock Statistics

The data used for the statistics provided in Table 17 utilizes the total BD, allowing for the inclusion of the organic layer samples. The data only includes the active layer. No extrapolations were made.

Table 17. Total active layer OC stock statistics

Floodplain	**Min (Mg C/ha)**	**Max (Mg C/ha)**	**Mean ± SE (Mg C/ha)**	**Median (Mg C/ha)**
LBC	23.45	387.04	131.28 ± 11.31	133.36
LRV	24.60	291.92	142.88 ± 8.44	138.31
LE	9.23	544.09	179.44 ± 14.88	163.63

7.6 Appendix F: Summary Statistics for Individual Mineral Samples

Table 18. Individual mineral sample carbon summary statistics across floodplains

		0.00-0.25	**0.25-0.5**	**0.5-0.75**	**0.75-1.0**	**1.0-1.25**	**>1.25**
		% Carbon	% Carbon	% Carbon	% Carbon	% Carbon	% Carbon
Min.	LBC	0.16	0.57	0.35	1.48	0.69	1.03
	LRV	0.19	0.56	1.07	0.06	0.26	0.21
	LE	0.27	2.06	0.63	0.44	0.26	0.34
Max.	LBC	18.21	18.16	10.62	11.30	7.18	6.64
	LRV	6.07	6.19	6.95	5.26	5.36	7.37
	LE	9.20	8.52	8.65	28.77	22.36	13.87
Median	LBC	5.53	7.92	3.69	3.96	3.89	2.52
	LRV	2.80	2.75	2.93	0.78	1.38	1.72
	LE	3.83	4.44	3.77	3.77	3.27	5.33
Mean	LBC	6.12	8.12	4.51	4.83	3.59	2.76
	LRV	2.95	2.89	2.91	1.45	1.91	2.45
	LE	4.14	4.78	3.88	4.88	5.88	5.42
Std. Dev.	LBC	5.26	4.14	3.11	2.61	1.75	1.40
	LRV	1.63	1.35	1.36	1.49	1.53	2.03
	LE	2.33	1.76	2.61	5.24	6.13	4.05